

ALMA MATER STUDIORUM · UNIVERSITÀ DI BOLOGNA

Scuola di Scienze

Corso di Laurea Magistrale in Fisica del Sistema Terra

Coastal altimetry for the computation of a Mean Dynamic Topography in the Mediterranean Sea

Relatore:

Prof. Nadia Pinardi

Presentata da:

Francesca Doglioni

Correlatore:

Dott. Jenny Pistoia

Dott. Paolo Cipollini

Sessione II

Anno Accademico 2016/2017

*Il percorso più breve tra due punti è una retta
L'ostacolo più inutile tra due punti è la fretta*

Jovanotti

Abstract

Satellite Sea Level Anomaly (SLA) observations are crucial in an operational oceanographic system due to their high coverage on sea surface currents and elevation and their strong constraint on water column integrated steric contributions. The use of Sea Surface Height (SSH) measurements by altimeter satellites in the Mediterranean Forecasting System (MFS) requires an accurate Mean Dynamic Topography (MDT) field with a high horizontal resolution which must be added to SLA observations. Here a new MDT computed through a *direct method* is proposed to solve the main limitations to the current MDT, evaluated from a model-dependent first guess. The *direct method* consists in the difference between an altimetric Mean Sea Surface Height (MSSH) and a geoid model. Moreover, a novel altimetric dataset reprocessed near the coast is adopted in order to improve the representation of coastal dynamics. Altimetric data from a single satellite, Jason-2, are used to generate a SSH dataset. This is used along with the EGM2008 geoid model to compute along track MDT observations. Optimal Interpolation algorithms are used to regrid along track MDT on MFS model grid. Derived geostrophic velocities are then computed. The validation of the altimetric dataset against the operational dataset showed improved performances in terms of time series completeness and standard mean error. From the analysis of the MDT and the retrieved geostrophic velocities we can conclude that the *direct method* allowed us to reconstruct basin scale and large scale MDT features but not meso/small scale and coastal dynamics. Main limitations in our results are due to the low accuracy of geoid model and the Jason-2 tracks spacing.

Sommario

Le osservazioni di Sea Level Anomaly (SLA) da satellite sono cruciali per un sistema operativo oceanografico in quanto forniscono un'estesa copertura delle correnti superficiali e dell'elevazione del livello del mare; inoltre costituiscono un forte vincolo per i contributi sterici integrati sulla colonna d'acqua. L'uso delle misurazioni di Sea Surface Height (SSH) da satellite all'interno del Mediterranean Forecasting System (MFS) richiede un campo di Mean Dynamic Topography (MDT) ad elevata accuratezza e risoluzione che deve essere sommato alle osservazioni di SLA. In questo lavoro si propone una nuova MDT, calcolata tramite un *metodo diretto*, per risolvere le principali limitazioni della MDT correntemente utilizzada in MFS, la quale è stimata a partire da un first guess dipendente dal modello stesso. Il *metodo diretto* consiste nella differenza tra una Mean Sea Surface Height (MSSH) altimetrica e un modello di geoide. Inoltre, si è adottato un recente dataset altimetrico, riprocessato nelle zone di costa, allo scopo di migliorare la rappresentazione della dinamica costiera. Dati altimetrici provenienti da un singolo satellite, Jason-2, sono stati utilizzati per generare un dataset di SSH. Questo, insieme al modello di geoide EGM2008, ha permesso di derivare osservazioni di MDT lungo le tracce del satellite. Algoritmi di Optimal Interpolation sono stati quindi utilizzati per ri-mappare le stime lungo traccia di MDT sulla griglia del modello MFS. Le corrispondenti velocità geostrofiche sono state calcolate a partire dai valori di MDT su griglia. Dall'analisi della MDT e delle velocità geostrofiche derivate, possiamo concludere che il *metodo diretto* ci ha permesso di ricostruire le caratteristiche della MDT a scala di bacino e su larga scala, ma non la dinamica costiera, di mesoscala e piccola scala. Le principali limitazioni nei nostri risultati sono legate alla scarsa accuratezza del modello di geoide e alla grande spaziatura fra le tracce di Jason-2.

Contents

1	Introduction	3
1.1	The Mediterranean Sea	5
1.2	The Mediterranean Forecasting System	7
1.2.1	Development phases	9
1.2.2	The model setup	9
1.2.3	Assimilated data: satellite altimetry	11
1.3	Thesis Objectives	13
2	Satellite altimetry for ocean forecast	15
2.1	Satellite observed quantities	15
2.2	From altimetric signal to Sea Surface Height	17
2.2.1	Principles of satellite altimetry	17
2.2.2	Altimeter signal and waveform analysis	19
2.2.3	Corrections	22
2.2.4	Data dissemination	24
2.3	Satellite altimetry and ocean dynamics	25
2.3.1	Methods of Mean Dynamic Topography computation	26
3	Sea Surface Height signal analysis	29
3.1	Data processing	29
3.1.1	Pre-processing	30
3.1.2	Target grid definition and 1 Hz averaging	32
3.2	Comparison with the operational Sea Level Anomaly dataset	34
3.2.1	Comparison of SLA datasets at original resolution	35
3.2.2	Comparison of SLA datasets on target grid	35
4	Mean Dynamic Topography computation and evaluation	43
4.1	Data and Methods	43
4.2	MDT features and geostrophic velocities	46
4.3	Discussion	51

CONTENTS

5 Conclusions and Outlooks	55
A Range and Geophysical Corrections	59

CONTENTS

Chapter 1

Introduction

Environmental scientific research aims to understand how natural processes work. In addition to investigating basic mechanisms, environmental sciences also aim to monitor and predict state variables systematically, since these data (including historical records) sustain basic research, such as climate related topics. Beyond the scope of scientific research, the information generated through monitoring and forecasting is of relevance because of its practical applications. For instance, decision making for the management of economic activities or emergency services relies on the knowledge of real-time and the forecast of near-future weather and ocean state (e.g., Jordi et al., 2006; Younis et al., 2008; Davidson et al., 2009; Chang et al., 2016).

Regarding Oceanographic Systems, given their complexity, realistic predictions are generated correcting numerical oceanographic model simulations via assimilation of direct observations. This goal is accomplished through the "operational" approach, i.e. with the centralized coordination of model development, maintenance of observational networks, and the implementation of data assimilation schemes (Pinardi and Coppini, 2010), all of which are guided by common objectives and plans. The combination of these activities is known as an Operational System.

The Mediterranean Forecasting System (MFS¹) is a regional operational system that was implemented in the late nineties (Pinardi and Flemming, 1998; Pinardi et al., 2003; Pinardi and Coppini, 2010; Tonani et al., 2014). The MFS routinely distributes maps of observed and predicted fields (e.g. Temperature, Salinity, Currents, Sea Surface Height), upon which more specific applications are based. On the MFS outputs is based the TESSA² project, which includes activities for the sea situation awareness (SeaCondition³, Coppini et al. (2017)) and other downstream

¹<http://medforecast.bo.ingv.it/>

²<http://tessa.linksmt.it/it/home>

³<http://www.sea-conditions.com/en/home>

services (e.g. safe and efficient routing, oil spill forecast, environmental quality indicators).

As any other operational system, the MFS consists of observational, model and data assimilation components, which are in continuous development (Demirov et al., 2003; Dobricic et al., 2005; Poulain et al., 2007; Tonani et al., 2008; Dobricic and Pinardi, 2008; Dobricic et al., 2012). The former includes in situ measurements and satellite data. Of the satellite data, Sea Level Anomaly (SLA) is one of the main variables used for assimilation; assimilation of SLA corrects the model representation of the small scale features of ocean circulation, besides having an effect also on Salinity and Temperature vertical profiles (Pujol et al., 2010).

SLA assimilation makes use of an estimate of the ocean Mean Dynamic Topography (MDT). The product currently used in MFS is the SMDT-MED-2014 (Synthetic Mean Dynamic Topography of the MEDiterranean sea) computed by Rio et al. (2014) and distributed by the Archivage, Validation et Interprétation de données des Satellites Océanographiques (AVISO).

Some issues about SLA assimilation by the MFS can be highlighted:

- The MFS does not assimilate SLA observations in areas where bathymetry is shallower than 150 m in order to avoid assimilation of data closer than 50 km from the coast (Adani et al., 2011). Altimetry observations are in fact generally considered not reliable in coastal areas (distance to the coast \leq 50 km) due to the corruption of signal by the nearby land (Gommenginger et al., 2011).
- The first guess of SMDT-MED-2014 is a long term average of the reanalysis produced from the MFS forecast itself (Adani et al., 2011). The intercalibration between different altimeters assimilated by the system makes the basin average of SLA close to zero. Hence the first guess used by Rio et al. (2014) is also offset toward zero, resulting in underestimated corrections of the model sea surface height. Moreover, since the MFS doesn't assimilate in coastal areas, the SMDT-MED-2014 first guess will be less accurate there.

In order to address the improvement of mean sea level representation in coastal areas and the need for an MDT totally independent from model simulations, a new MDT in the Mediterranean Sea is computed in this work starting from a novel coastal altimetric dataset.

The following sections of this introductory chapter describe the geography and the main circulation features of Mediterranean Sea, along with an overview of the

1. The Mediterranean Sea

MFS operational system. Finally, details about the objectives of this thesis will be given.

1.1 The Mediterranean Sea

The Mediterranean Sea is a mid-latitude semi-enclosed sea, situated between latitudes 30° N and 46° N with a zonal extension between 6° W and 37° E. It is characterized by anti-estuarine circulation with a net heat and fresh water loss at the sea-air interface, being balanced at multidecadal time scales by the inflow of Atlantic Water from the Gibraltar strait, at the westernmost extreme. The bathymetry depth varies within a relatively large range, alternating some shelf areas such as the Adriatic Sea and the Tunisian shelf, having depth under 100 m, to deep ocean areas such as the Tyrrenian Sea, the Ionian Sea and some areas of the Levantine Sea reaching 4000-5000 m. The basin is delimited by three shallow straits: the Gibraltar Strait, having maximum depth of 300 m; the strait of Sicily, that reaches a maximum depth of 500 m and divides the Mediterranean into its two main sub-basins of comparable size, The Western Mediterranean (WMED) and the Eastern Mediterranean (EMED) (Fig 1.1); the Dardanelles, having maximum depth around 100 m and separating the Mediterranean from the Marmara Sea and the Black Sea.

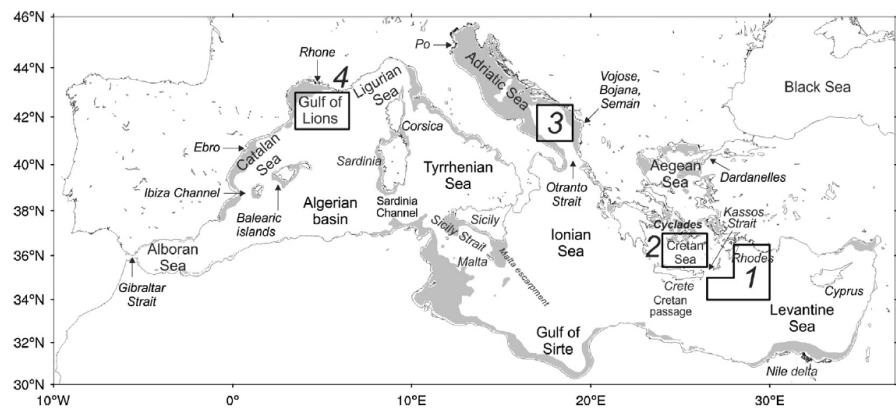


Figure 1.1: Mediterranean basin geometry and main sub-basins; the shaded areas indicate depths less than 200 m. Reproduced from Pinardi et al. (2015)

Despite the relatively small size of this basin, all ocean circulation scales are present in the Mediterranean Sea: a synoptic scale circulation belt, sub-basin scale gyres and jet-like structures and a mesoscale and sub-mesoscale eddy field.

The general thermohaline circulation is prompted by the water inflow at the Gibraltar Strait and is maintained by deep and intermediate water masses formation induced by large freshwater fluxes and intense winter heat fluxes at surface (Adani

et al., 2011). The Mediterranean conveyor belt is constituted by a shallow zonal and two deep meridional circulation belts; current branches flowing at different depths are linked within regions of intermediate and deep water masses formation (Pinardi and Masetti, 2000). The shallow Atlantic Water (AW) stream entering from the Strait of Gibraltar flows all through the basin toward the Levantine Sea, where it transforms into the Levantine Intermediate Water (LIW) (Fig. 1.2). The intermediate depth flow emanates from the Rodhes Gyre region, directed toward west. LIW separates into three main branches: one generating the recirculating outflow at the Strait of Gibraltar and two others constituting the upper part of the two meridional cells, of which one is situated in the WMED an the other in the EMED. The thermohaline circulation of these two cells is driven by deep water masses formation happening respectively in the Gulf of Lion and in the Adriatic sea and sustained by the presence of LIW, which contributes to the salt budget.

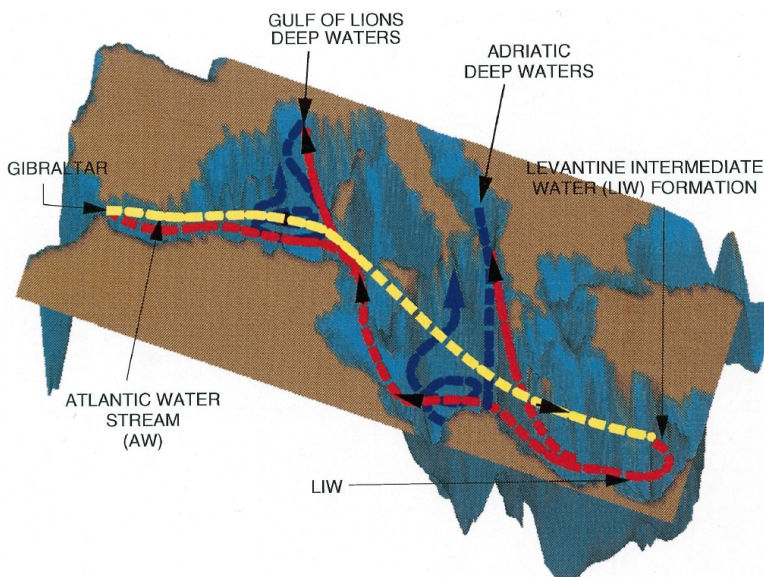


Figure 1.2: Schematic of Mediterranean Conveyor Belt system. Reproduced from Pinardi and Masetti (2000)

Surface circulation at the sub-basin scale is characterized by semi-permanent gyres, coastal currents and free jets. At the basin scale, these patterns form a meridional double gyre structure, driven mainly by the wind stress, dominated by the Mistral westerly jet during winter and the Etesian North-easterly jet during the summer (Pinardi et al., 2015). This forcing induces northern cyclonic gyres associated with positive wind stress curl (e.g. Lions Gyre, Tyrrenian Gyre), and southern anticyclonic gyres associated with negative wind stress curl (e.g. Syrte Gyre, Tyrrhenian Gyre) (Fig. 1.3).

Persistence of an eddy field is observed in the Mediterranean Sea, which is

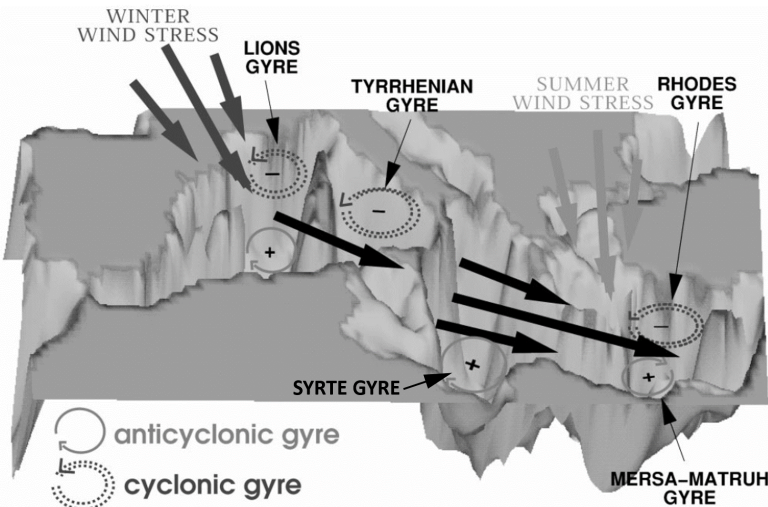


Figure 1.3: Double gyre structure of surface circulation induced by wind stress. Reproduced from Pinardi and Masetti (2000)

thought to be determined by the specific local atmospheric forcing, the complex bathymetry and the strong non linear dynamics associated with a short Rossby radius of 10 km (Iudicone et al., 1998; Pinardi et al., 2015).

1.2 The Mediterranean Forecasting System

Operational Oceanography has been implemented in the Mediterranean Sea since the late nineties with the development of the Mediterranean Forecasting System (MFS). The MFS is an observing and modelling system which provides oceanographic forecast, analysis and reanalysis for the physical and biogeochemical parameters of the Mediterranean Sea at a basin and regional/shelf scale.

The components of the forecasting system are maintained by research groups dislocated in different institutions. Some research institutions are in charge of maintaining the observational network and analysing incoming data (e.g. Istituto Nazionale di Oceanografia e Geofisica Sperimentale (OGS), Centro Nazionale delle Ricerche-Istituto delle Scienze dell'Atmosfera e del Clima (CNR-ISAC), Collecte Localisation Satellites (CLS)). In situ instruments state is constantly monitored by these groups, which also process and quality-control satellites and in situ data to generate datasets used in the forecast production chain. Besides, the systematic assessment of the network efficiency and costs aids the planning of new deployment programs, in a continuous improvement process (Poulain et al., 2007).

Other research groups produce forecasts, analysis and reanalysis of physical and biochemical variables (e.g. Istituto Nazionale di Geofisica e Vulcanologia (INGV),

2. The Mediterranean Forecasting System

Centro Euro-Mediterraneo sui Cambiamenti Climatici (CMCC), OGS). Numerical models are configured according to the characteristics of the specific region of interest, continuously improving the domain and resolution, bathymetry and coastlines, sub-grid parametrizations such as diffusion coefficients, atmospheric forcing (e.g. Kourafalou and Tsiaras, 2007; Tonani et al., 2008; Oddo et al., 2009). Upgrades of data assimilation schemes are performed coherently to observational and modelling components evolution. The ability of the system to integrate observations is constantly increased with the introduction of new techniques and ad hoc tunings (Dobricic et al., 2007; Adani et al., 2011).

Forecast of the physical variables at the basin scale is currently maintained by the Mediterranean-Monitoring and Forecasting Centre (Med-MFC) subgroup, having its headquarters at Istituto Nazionale di Geofisica e Vulcanologia (INGV) in Bologna. The forecast production chain consists in a daily simulation and data assimilation cycle which produces hindcasts used then to initialise the next model run (Fig. 1.4); the forecast is initialized by a hindcast every day except Tuesday, when the analysis is used (INGV technical report, Delrossi et al., 2016). One week analysis is released once a week, while ten-day forecast is produced every day. Analysis and forecast products are available in real time to the users through a dedicated ftp service and every day a web bulletin is published on the web site: <http://medforecast.bo.ingv.it/>.

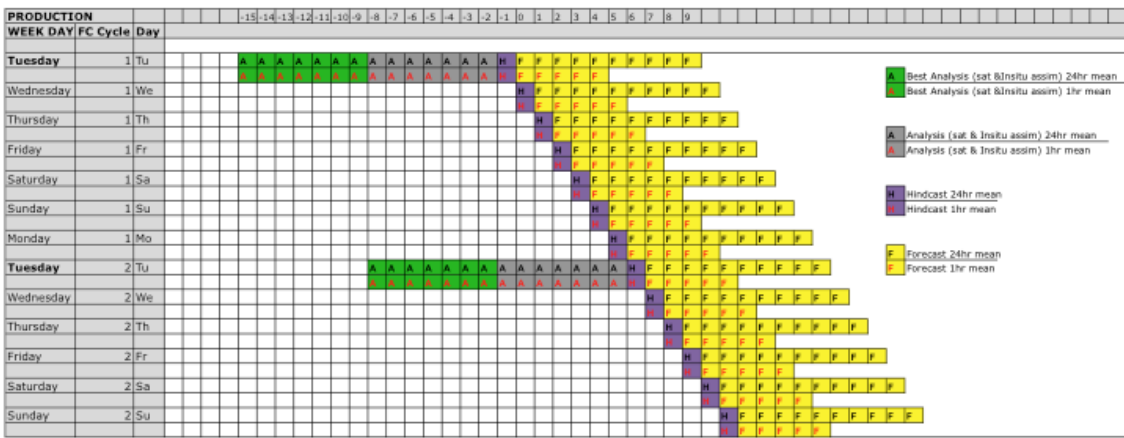


Figure 1.4: Forecast production chain (taken from <http://medforecast.bo.ingv.it/system/>). Ten-day forecast is produced initialized by a hindcast every day except Tuesday, when the analysis is used.

In addition to the basin-scale system, some high resolution models have been developed which are one-way nested into the MFS. They use daily means fields computed from daily outputs of the coarse general circulation model. Some of these regional systems, working specifically in the Italian seas (Adriatic, Ionian and Tyrrhenian basins), are part of the Ocean-Lab project (<http://oceanlab.cmcc.it/>).

2. The Mediterranean Forecasting System

Ocean-Lab supports all the steps of the production chain, from data gathering and model development to the distribution of forecasting products through the implementation of user-friendly interfaces.

1.2.1 Development phases

The MFS implementation and pre-operational testing was realised in two phases: the Mediterranean Forecasting System Pilot Project phase (MFSPP, developed in the period 1998-2001, Pinardi et al. (2003)) and the Mediterranean Forecasting System Toward Environmental Prediction phase (MFSTEP, realised in 2003-2006, Pinardi and Coppini (2010)). These two phases mainly developed the hydrodynamic modelling of waves and currents and the monitoring and prediction of physical state variables. Simultaneously, the necessity existed to explore the potential predictability of the marine ecosystem through the consideration of other marine state variables (biogeochemical fields). This goal was achieved within the framework of the Global Ocean Observing System (GOOS, 1997), which supported ecosystem modelling through the development of an observing system within a regional alliance for the creation of the Mediterranean Global Ocean Observing System (MEDGOOS, 1999) and the Mediterranean Operational Oceanography Network program (MOON, 2005), at a later time melded in the Mediterranean Operational Network for the Global Ocean Observing System (MONGOOS⁴, 2012).

Operational oceanography in the European seas have been supported in recent years by the European projects MyOcean(2009-2012), MyOcean2 (2012-2014) and MyOcean Follow-On (2014-2015). At present the demonstration phases carried on during the MyOcean projects have ended in the broader pan European Copernicus - Marine Environment Monitoring Service (CMEMS⁵). MFS products at the basin scale are collected and distributed in the CMEMS online catalogue (<http://marine.copernicus.eu/services-portfolio/access-to-products/>).

1.2.2 The model setup

The purpose of the model in the MFS forecast production chain is to provide a first guess of the ocean state as accurate as possible. New processes and setups are introduced to gradually improve its physical coherence (e.g. (Oddo et al., 2009, 2014)).

The MFS numerical modelling at the basin scale is based on the hydrodynamic

⁴<http://www.mongoos.eu/home>

⁵<http://marine.copernicus.eu/>

2. The Mediterranean Forecasting System

model Nucleus for European Modelling of the Ocean (NEMO), coupled with the wave model WaveWatch-III (WWIII). Solutions of the NEMO system of primitive equations are three-dimensional fields of zonal, meridional and vertical velocities (u, v, w), temperature T , salinity S and pressure P . In addition, a two dimensional sea surface height field η is included, modelled at present through the ‘free surface’ formulation (Tonani et al., 2008). In the free surface formulation the pressure at a certain depth z_0 is given by the contribution of three terms:

$$P(z_0) = \rho_0 g \eta + P_0 + \int_{z_0}^0 \rho g \cdot dz \quad (1.1)$$

where the first term is the pressure due to the free sea surface displacements, η , P_0 is the diagnostic distribution of pressure over a rigid lid at $z = 0$ and the last term is the hydrostatic pressure. η is given by the solution of a prognostic equation, defined by the vertical average of the surface boundary kinematic condition:

$$\frac{\partial \eta}{\partial t} = -\bar{U}_h \cdot \nabla(\eta + H) + P - E \quad (1.2)$$

where \bar{U}_h is the horizontal velocity vector, i.e. $\bar{U}_h \cdot \nabla(\eta + H)$ is the horizontal advection of water mass, and $P-E$ is the vertical volume flux of fresh water (the precipitation minus evaporation budget). The reference surface ($z = 0$) for η represent the ideal state of rest of the ocean, i.e. the geoid.

Assumptions are made in the primitive equations formulation, based on scale considerations: Boussinesq hypothesis, hydrostatic hypothesis, thin shell approximation, spherical Earth approximation, incompressibility hypothesis, turbulent closure hypothesis. The model output consists of daily mean fields of temperature, salinity, currents, sea surface height, wind stress, heat flux, water flux, and short-wave radiation (Adani et al., 2011).

NEMO is currently configured by the MFS for the Mediterranean Sea with horizontal regular resolution of 1/16 of a degree and 72 unevenly spaced vertical levels. A set of limited area forecasting models are nested in different sub-regional and shelf areas on the large scale system (Pinardi and Coppini (2010)). A portion of model domain in the Atlantic ocean is nested within a global ocean general circulation model in order to improve the representation of the inflowing Atlantic water properties (Oddo et al., 2009). The three dimensional domain is defined by the surface and bottom boundaries. Momentum, water and heat fluxes are computed through these boundaries by bulk formulas, using as input operational analyses from the European Centre for Medium-range Weather Forecast (ECMWF) (Tonani et al., 2009).

2. The Mediterranean Forecasting System

The water balance is computed as Evaporation minus Precipitation and Runoff, including the Dardanelles inflow parametrized as a river (Delrosso et al., 2016).

Since the model is not perfect and the initial conditions are affected by error, simulations tend to diverge from the real ocean state as the integration time flows. Hence, the production of good forecasts relies on the intermittent correction of the simulations through the integration of observations.

1.2.3 Assimilated data: satellite altimetry

A variational data assimilation scheme (3DVAR) is the component of the MFS which constrains the model output through observations, improving the realism of the model fields. The assimilation cycle consists in the minimization of a cost function constructed with the misfits between observations and the numerical simulation (Dobricic and Pinardi, 2008). Misfits are then used daily to correct the forecast and initialise the following run with the corrected state.

Observations assimilated by the MFS consist of in situ temperature profiles by VOS XBTs (Voluntary Observing Ship-eXpandable Bathymeterograph), in situ temperature and salinity profiles by Argo floats and CTD (Conductivity-Temperature-Depth), Sea Level Anomalies (SLA) derived from satellite altimetry and satellite Sea Surface Temperature (SST) data used for the correction of surface heat fluxes (Petenuzzo et al., 2010).

- * XBTs are in situ instruments composed by hand launchers, data processing/recording devices and expendable probes. They are used for the collection of single profiles of Temperature and are deployed from routine Volunteer Observing Ships (VOS). Data are transmitted through the Global Telecommunication System to the MFS-VOS data centre ENEA, La Spezia, where they are processed and distributed.
- * Argo floats are freely-drifting instruments collecting vertical profiles of physical, biogeochemical and optical data. MedArgo are units specifically designed to be deployed in the Mediterranean Sea (Poulain et al., 2007). Their maximum profile depth alternate between 700 m and 2000 m, and an intermediate "parking depth" of 350 m has been chosen to be close to the LIW core. They are equipped with CTD sensors which provide the MFS with T and S profiles. MedArgo data are transmitted through the Argos satellite system and processed both by the MedArgo Thematic Expert Data Centre (TEDC) at OGS in Trieste and by the CORIOLIS Operational Oceanography Data Cen-

2. The Mediterranean Forecasting System

tre, which perform a first data quality control. Observations are available in near-real time within a few hours of the actual measurement.

- * Heat exchanges with the atmosphere depend on the SST. For an accurate computation of surface heat fluxes, the Temperature of the MFS first model layer is relaxed toward satellite SST maps (Pettenuzzo et al., 2010). Night time observations are obtained from Advanced Very High Resolution Radiometer (AVHRR) measurements, optimally interpolated as described in Marullo et al. (2007) on the MFS grid and distributed in near-real time by the Istituto di Scienze dell'Atmosfera e del Clima - Gruppo di Oceanografia da Satellite (ISAC-GOS).
- * SLA from three satellites is assimilated by the MFS: Jason-2, Cryosat-2 and SARAL/AltiKa (Fig. 1.5). The SLA Tailored Altimetry Products for Assimilation Systems (TAPAS) dataset is used, computed by the Sea Level Thematic Assembly Center (SL-TAC) and distributed through the Copernicus Marine Environment Monitoring Service (CMEMS). SLA TAPAS are datasets specifically created to give the possibility to the end user to add back the contribution of tides and the effect of atmospheric pressure which are usually removed from the observed sea level. The sea level variations due to atmospheric pressure are added to SLA TAPAS before assimilation since this forcing is included in the MFS modelling (Dobricic et al., 2012).

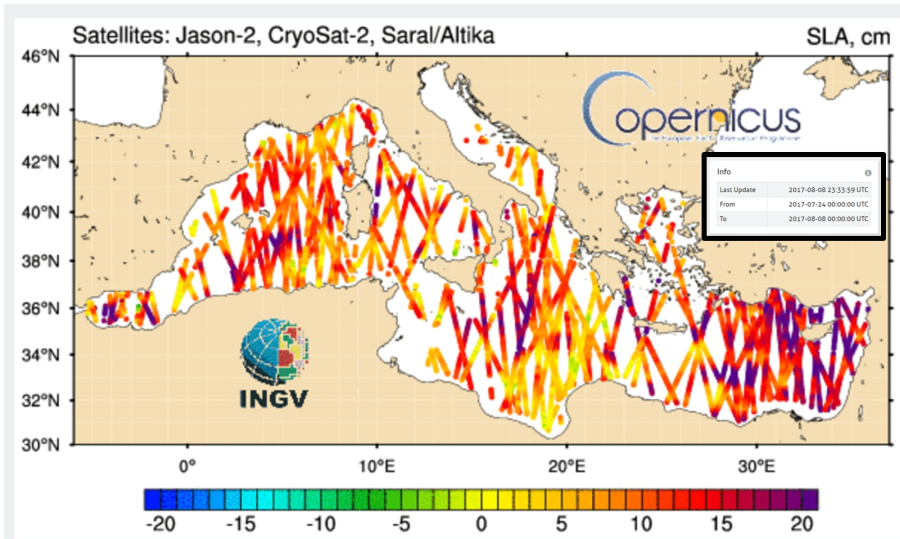


Figure 1.5: SLA observations assimilated by the MFS between the 7th and the 8th of August 2017. The map is taken from the MFS bulletin (<http://medforecast.bo.ingv.it/assimilated-data/>).

3. Thesis Objectives

The development of satellite altimetry in the latest decades has been one of the revolutions in oceanography. Together with the implementation of Argo, it has contributed to construct a global system of uniform and three dimensional observations available in real-time, which is extremely important for operational oceanography.

According to Pujol et al. (2010), in the Mediterranean Sea the assimilation of SLA observations by multiple altimeters reduces the Root Mean Square Differences (RMSD) between analysis and observations of some tenth percent in comparison with the RMSD between model simulations without assimilation and observations. In this sea, satellite altimetry is particularly efficient for the characterization of the two dimensional horizontal structure of the chaotic eddy field (Iudicone et al., 1998). Eddies position, shape and intensity are difficult to accurately predict without an observational constraint. This is particularly important in regions of intense variability, for instance in the Alboran, Algerian, Southern Ionian and Levantine Basins (Iudicone et al., 1998).

The prevalent meso/small scales of the Mediterranean circulation patterns and the MFS model high horizontal resolution (at present a 6-7 km regularly spaced grid) demand a dense observational dataset (Oke et al., 2015). Given the broad distance between tracks of some satellites (e.g. TOPEX/Poseidon (T/P), Jason 1 (J1) and 2 (J2)) or the long repetition period for others (e.g. Envisat), multisatellite datasets are needed to increase mapping capabilities (Pascual et al., 2007; Pujol et al., 2010); ground tracks of the T/P-J1-J2 satellite, for instance, are not able to detect the Rhodes Gyre since it is positioned in between the mesh (Iudicone et al., 1998).

Similarly, gaps in the coverage of coastal areas limit the detection of circulation features over the shelves (see, for instance, the Liguro-Provencal-Catalan Current intrusion events in the Gulf of Lion, Bouffard et al. (2011)). Despite their importance for human activities and settlements, coastal areas are still under-observed by satellites. Since rapid changes in the sea level and small scale features are present in these areas, progresses in observation recovering there are crucial.

1.3 Thesis Objectives

The aim of this thesis is to investigate the capability of a novel altimetric dataset re-processed in coastal areas to describe Mean Dynamic Topography (MDT) features in the Mediterranean Sea. We first approach satellite data analysis and processing and then evaluate the resulting mean ocean topography and circulation by comparison with other products and reconstructions from the literature.

The main objectives are three:

3. Thesis Objectives

1. Computation of a Sea Surface Height dataset along Jason 2 tracks over the Mediterranean for the period from 2008 to 2015 using a novel altimetric Coastal Geophysical Data Record (CGDR). The coverage and quality of this dataset in coastal areas is evaluated by comparison with the SLA TAPAS dataset.
2. Computation of an along track Mean Dynamic Topography using the sea surface height dataset created, together with a high resolution geoid model; construction of a MDT map through optimal interpolation on the MFS homogeneous horizontal grid.
3. Analysis of the mean circulation for MDT calculating the surface geostrophic velocities.

Chapter 2

Satellite altimetry for ocean forecast

In this chapter we will give an overview of main space-borne observations used for ocean forecasting and their role in the identification of ocean circulations. We will focus on altimetric observations, explaining how their information on sea surface topography is derived and highlighting coastal areas problems. In the final part we will describe sea surface height components and the available methods for the computation of the mean dynamics.

2.1 Satellite observed quantities

Satellite observations are a fundamental component of operational oceanography. They are processed and made accessible in near-real time, providing the forecast chain with the latest information on the sea state. Active and passive sensors mounted on board of satellites provide continuous, global and spatially homogeneous observations of the sea surface. This makes them complementary to in situ observations which are sparse, inhomogeneous and provide information on the vertical structure of the water column.

Surface horizontal currents and vertical motions are forced by exchanges of momentum and heat at the air-sea interface. These exchanges can be indirectly observed through remote sensing of the sea surface properties (sea level, temperature, roughness). Since model equations are driven by atmospheric forcings, assimilation of satellite observations enhance forecast realism. If we consider a steady state, main components of surface currents are the geostrophic and Ekman velocities, which are connected to the deep circulation by deep water mass formations.

Geostrophic velocities result from the balance of atmospheric pressure gradient

forces and Coriolis forces. If we assume hydrostatic equilibrium, pressure at the sea level is related to the sea surface displacement η and horizontal velocities derive from:

$$\begin{cases} u = -\frac{g}{f} \frac{\partial \eta}{\partial y} \\ v = \frac{g}{f} \frac{\partial \eta}{\partial x} \\ \frac{\partial P}{\partial z} = -\rho g \end{cases} \quad (2.1)$$

where g is the gravity acceleration and $f = 2\Omega \sin(\varphi)$ is the Coriolis frequency (with φ latitude and $\Omega = 7.29 \cdot 10^{-5} \text{ rad/s}$). Excluding the equatorial strip, geostrophic balance and hydrostatic equilibrium describe with good approximation the surface ocean circulation on spatial scales bigger than some tenth of kilometres and time scales longer than a few days. Large scale circulation is hence well described by the Sea Surface Height field (SSH), remotely observed by active instruments called altimeters. Other effects that contribute on altimeter heights are the seasonal steric expansion and contraction of the water column, the oceanic and solid earth tides and the local transient pressure variations due to the wind at surface.

In the Ekman balance, the Coriolis force is balanced by the vertical divergence of wind stress, and the induced velocity profile has the shape of a spiral decaying with depth. The intensity of Ekman currents at surface depend on the intensity of wind stress τ_0 acting on the surface. Wind signature on surface roughness allows to retrieve wind speed from ocean backscatter coefficient measured through active instruments (scatterometry, Bourassa et al., 2010). Active and passive instruments are also used to retrieve wind direction. These observations are used in the Ocean Surface Current Analyses Real-time (OSCAR) project, which reconstructs surface currents based solely on satellite fields (Dohan, 2017). Quikscat surface wind observations are at present used by the MFS to correct the operational ECMWF outputs used to force the model (Pettenuzzo et al., 2010).

Sea Surface Temperature (SST) is another important quantity observed from space. Given the emissivity ϵ_λ of the ocean surface at a certain wavelength, the black body radiation emitted E_λ is related to the SST (T_s) by the Stefan-Boltzmann law:

$$E_\lambda = \epsilon \sigma T_s^4$$

where σ is the Stefan–Boltzmann constant. Passive instruments called radiometers are used on board of satellites to measure radiation at different frequencies and combine them linearly to determine SST minimising the influence from atmospheric refraction and emission. Observations assimilated by the MFS are obtained from night-time Advanced Very High Resolution Radiometer (AVHRR) measurements,

optimally interpolated as described by Marullo et al. (2007). This IR instruments sense radiation emitted by the 10-micron thin skin of the ocean, which is in direct contact with the atmosphere. Maps obtained from AVHRR measurements are used in the MFS as relaxation fields for the first model layer, in order to correct surface heat fluxes.

2.2 From altimetric signal to Sea Surface Height

Since satellite altimetry is a remote sensing technique, the signal received back by the sensor includes many undesired information and biases due to interactions with the atmosphere and to the way the signal is reflected by the surface. The extraction of the topographic signal from the returned echo is not straightforward since it relies on the development of techniques for noise reduction, fitting algorithms and external products for the exclusion of the undesired signals. In this section we will see how the raw signal sensed by the altimeter is processed in order to be turned into a SSH estimate.

In this work we will make specific reference to some characteristics of Jason 2 satellite (J2). This satellite is part of the Jason mission series (Topex/Poseidon, Jason-1, Jason-2 and the recently launched Jason-3) which has become a reference for all satellite altimeters because of their precision and their long term continuity. Among the Jason missions, J2 was chosen for this work because it was the only one re-processed near the coasts with the ALES algorithm at the time this work was performed.

2.2.1 Principles of satellite altimetry

Satellite radar altimeters are active instruments which send intermittent pulses to the surface and retrieve information on it analysing the shape of the returned echo (hereafter *waveform*). The aim of satellite altimetry is the observation of ocean topography for the investigation of large scale ocean circulation at the surface. Nevertheless, waveform analysis reveals also statistics that characterize the sea state and surface roughness.

The two-way travel time of the pulse reflected by the earth surface gives an estimate of its distance from the satellite (hereafter *range*). Range varies in space and time due both to variability of sea surface and to variation of the distance of satellite from the centre of mass of the Earth, which is its orbit. The observed range is derived assuming that the pulse is travelling at the speed of light in the vacuum. Some corrections are needed to account for the presence of atmosphere and

2. From altimetric signal to Sea Surface Height

other effects. Instantaneous ocean topography is obtained by subtracting the range measurement from the value of the orbit at the time of measurement (see Fig. 2.1).

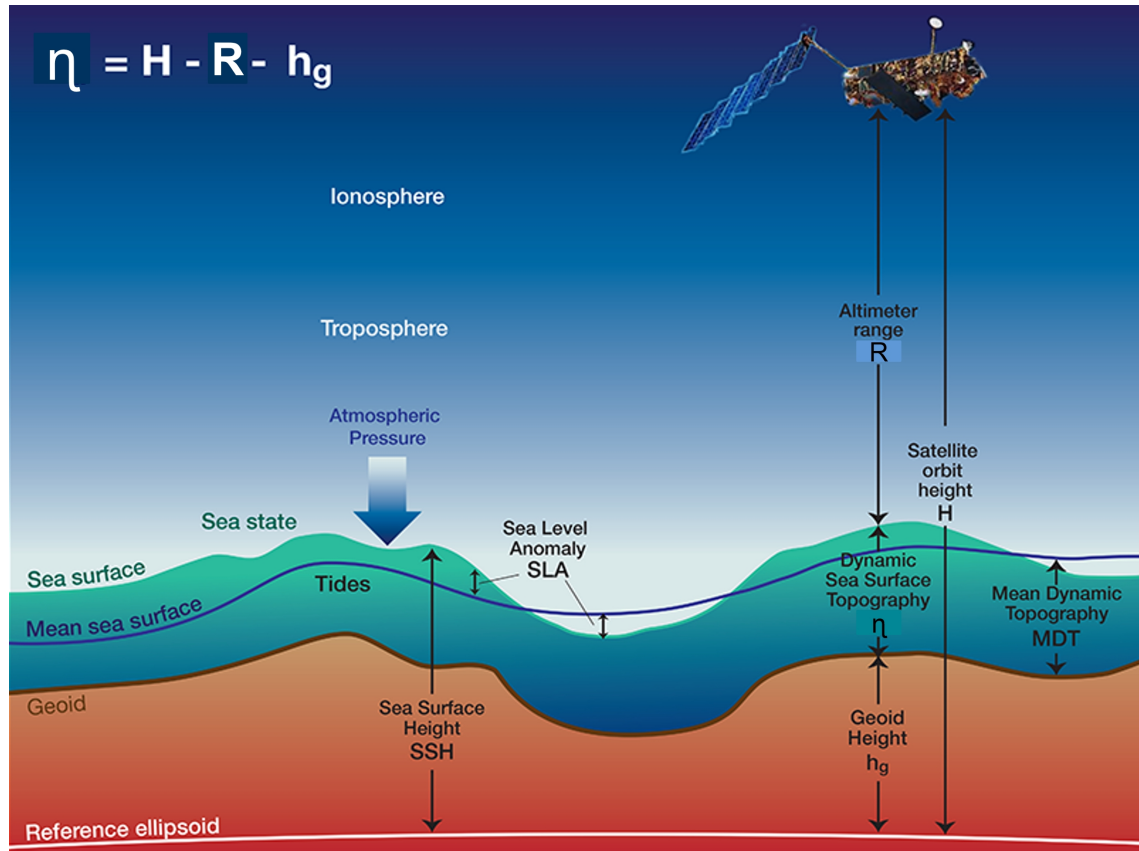


Figure 2.1: Components of the sea surface height as observed by satellite altimetry (image taken from <http://www.learn-eo.org/resources.php>).

The along-track range (R_{obs}) and the relative corrections (ΔR) together with the satellite orbit (H), result in the computation of the SSH as:

$$SSH = H - (R_{obs} + \Delta R) \quad (2.2)$$

This basic principle relies on the successful analysis of the altimetric waveforms and on the correction of the observed range R_{obs} from external perturbations. Despite altimetry is quite successful in open ocean, in the coastal areas satellite altimetry data processing and interpretation has specific difficulties, for example the interaction of the radar signal with land topography, inaccuracies in some of the corrections and fast changes in the sea level. Thus dedicated re-implementations of the complete processing chain up to the computation of SSH are required (Roblou et al., 2007).

Given the amount of coastal observations that for these reasons remain unused in the archives, the need for agreement on methods for the extension of altimetry

2. From altimetric signal to Sea Surface Height

databases to the coastal zones has been acknowledged since the turn of the century (Anzenhofer et al., 1999). Nowadays the exploration of new techniques is supported by major space agencies and coordinated through a series of research projects (e.g. COASTALT¹, PISTACH (Mercier et al., 2010), RECOSETO²). Namely, the aim of Coastal Altimetry is to develop new algorithms to fit the altimetric signal and find new strategies to determine corrections in coastal areas.

2.2.2 Altimeter signal and waveform analysis

The *Poseidon* altimeters mounted on board of the Jason satellites series are characterized by the ‘pulse limited’ technology (Fig 2.2). The emission power is concentrated in a short time, in order to generate a beam with spanning angle large enough to compensate for mispointing of satellite (Chelton et al., 2001).

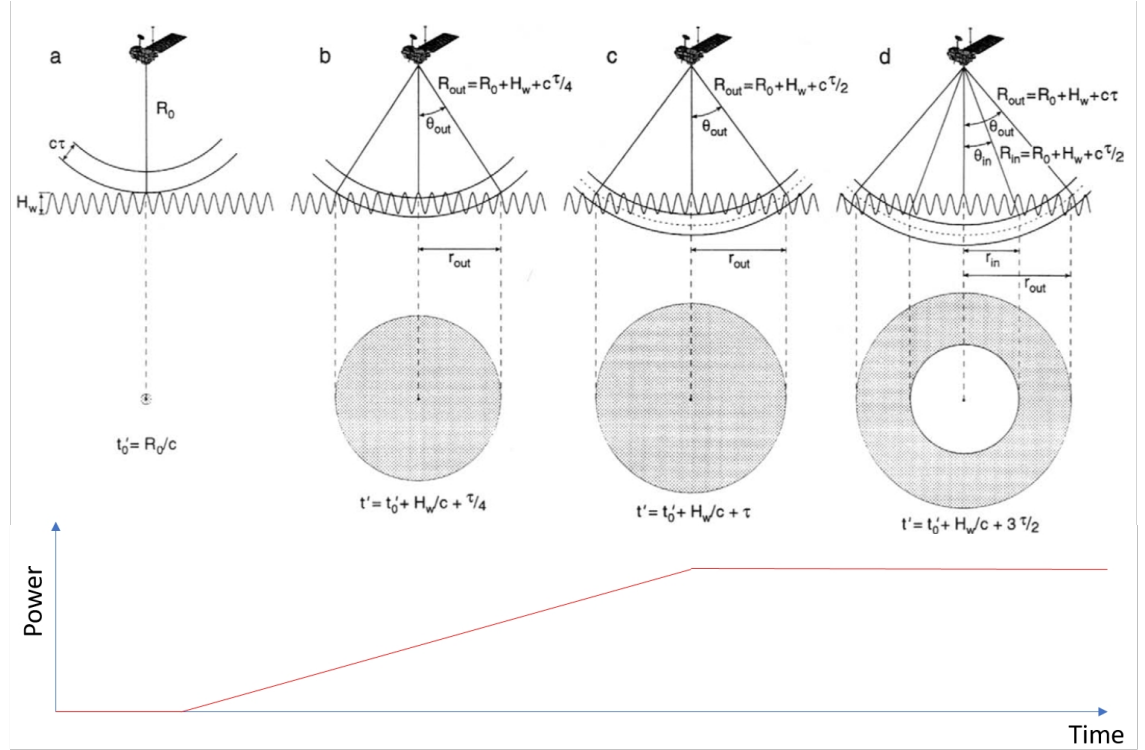


Figure 2.2: Illustration of radar pulse propagation at the ground for a ‘pulse limited’ altimeter. In the bottom panel is shown the return power correspondingly detected by the altimeter sensor in the ideal case. Modified from Chelton et al. (2001).

The footprint has a maximum diameter varying between 2 and 10 km, depending on the sea state. The altimeter sensor registers the instantaneous power reflected within the footprint as function of time (or ‘gates’). Hence the power detected at

¹<http://www.coastalt.eu/>

²http://www.geodesy.tu-darmstadt.de/psg/projekte/recoseto/projekte_recoseto.en.jsp

a certain gate depends on the reflectivity of the surface at a radial distance from the nadir proportional to the gate number. Since at the original pulse repetition frequency (thousands per second) waveforms are too noisy to be analysed, groups of single waveforms are averaged out in real time before the transmission from satellite to the ground (Fig 2.3, right panels). Generally, data at a sampling frequency of some tenth of Hz (10-40 Hz) obtained averaging groups of 100 waveforms are transmitted to the ground. This correspond to a 10 times reduction of noise given that the measurement error falls as the square root of the number of observations. The returned waveform for open-ocean measurements is schematically shown in the left panel of Fig 2.3.

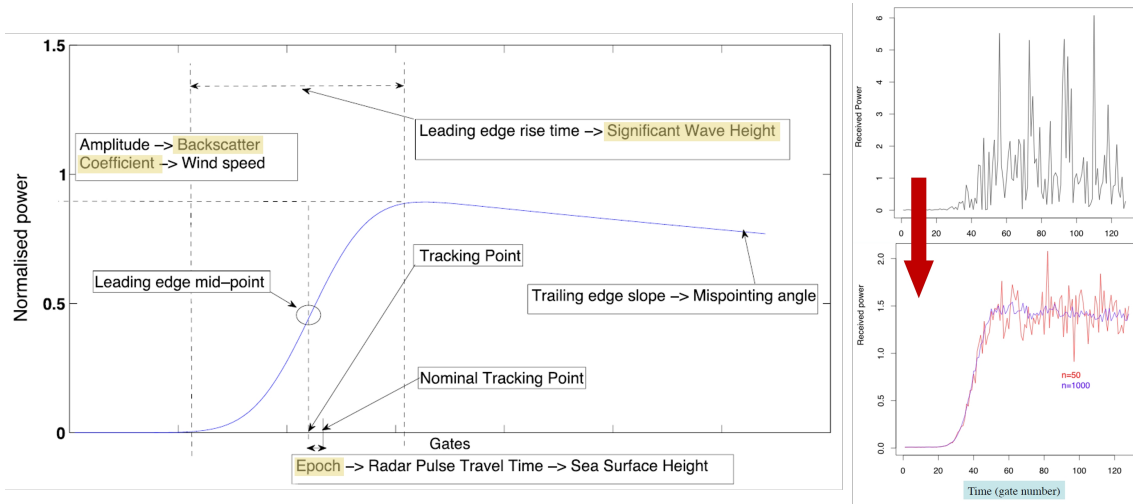


Figure 2.3: Left panel: schematic of the returned waveform detected by altimeter sensor over open ocean; main parameters estimated from interpolation are highlighted. Reproduced from Passaro et al. (2014). Right panels: waveform detected at the original pulse repetition frequency (\approx kHz, top) and signal obtained after averaging out respectively groups of 50 and 1000 waveforms (bottom). Reproduced from Cipollini and Snaith (2015).

The processing step which retrieves geophysical information from the waveform is called *retracking*. The retracking process consists of fitting a model response to the real waveform. Over the open ocean, most waveforms are well described by the Brown mathematical model (Brown, 1977), which is the standard model used for the retracking of three (sometimes four, depending on the algorithm) parameters (Passaro et al., 2014):

- the epoch, linked to the travel time of radar pulse and hence to the sea surface height;
- the amplitude of signal, used to retrieve backscatter coefficient (σ_0) of ocean over the footprint and hence the wind speed at the surface;

2. From altimetric signal to Sea Surface Height

- the leading-edge rise time, depending on the Significant Wave Height (SWH) over the footprint;
- (-) the slope of the trailing-edge, linked to the mispointing angle of the satellite radar beam.

Epoch is used to study ocean topography, backscatter coefficient to study surface winds and SWH for ocean waves monitoring. Epoch is converted in the two-way travel time τ , which is used to compute the observed range R_{obs} assuming that the radar pulse travels at the velocity of light in the vacuum c_0 :

$$R_{obs} = \frac{c_0 \cdot \tau}{2}$$

However, the classical Brown functional form is no more valid when waveforms are corrupted by the presence of 'bright targets' in the satellite footprint, which are objects whose reflectivity is much higher than the surrounding ocean surface (e.g. ships, calm patch of water, land). The corruption happens in particular in the last 10 km from the coastline and returned echoes take various shapes (Fig 2.4). The waveforms that cannot be fully retracked by the Brown analytical form are generally discarded.

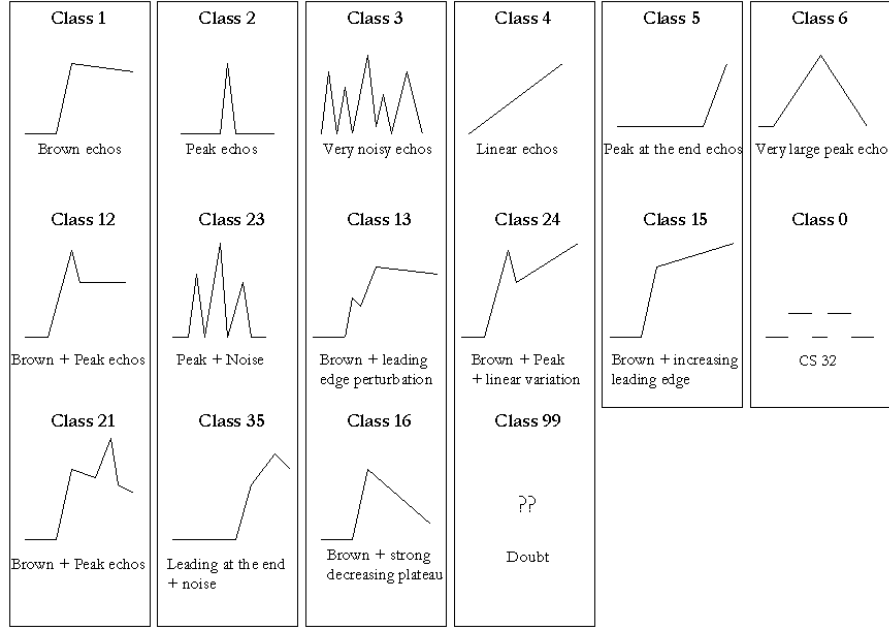


Figure 2.4: Schematic representation of the waveforms classes (taken from <https://www.aviso.altimetry.fr/fr/donnees/information-sur-les-produits/information-about-mono-and-multi-mission-processing/specific-processing/processing-for-coastal-and-hydrology-products-pistach.html>).

Retracking strategies are either empirical or derived from theoretical knowledge

of scattering. Innovative retracking techniques for the detection of bright targets in coastal areas are continuously emerging: peaks are identified either treating each waveform independently with iterative methods or through multi-waveform approaches that extract information on the bright target signature from batches of waveforms (see Fig 2.5, Gommenginger et al., 2011; Passaro et al., 2014).

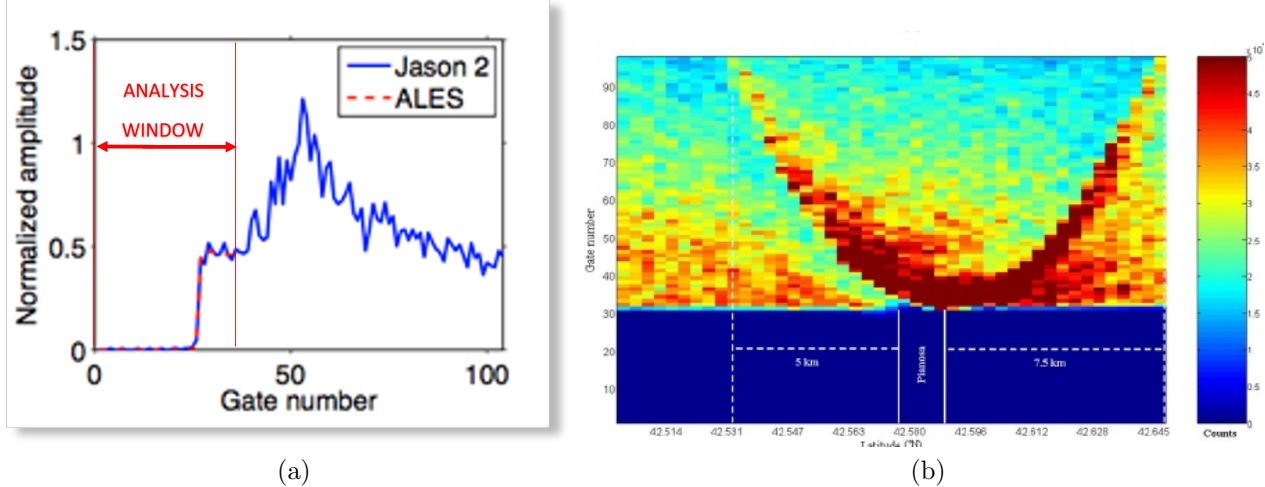


Figure 2.5: Strategies for retracking of corrupted waveforms: (a) an iterative method is used to identify the peak and adapt the width of analysis window (modified from Passaro et al. (2014)); (b) the parabolic signature of the bright target can be identified from a multi-waveform analysis (reproduced from Gommenginger et al. (2011)).

2.2.3 Corrections

Altimeters mounted on board of satellites use radiation in the microwave band in order to minimize the absorption and scattering by atmospheric elements. For instance, the Poseidon 3, on board of J2, is a bi-frequency altimeter with principal and secondary emission frequencies at 13.6 GHz and 5.3 GHz respectively (Dumont et al., 2016). In Fig 2.6 the spectrum of transmissivity of various kind of atmospheres is shown as reference.

Sources of residual error affecting the range estimate can be divided into two categories, described in the following:

- *Range corrections* account for the path delay due to the presence of dry gases (ΔR_{dry}) and water vapour (ΔR_{wet}) in the troposphere, and free electrons in the ionosphere (ΔR_{iono}), which slow down and attenuate the radiation. Rain events damp and distort the signal much more than all other atmospheric wet components; for this reason measurements contaminated by the presence of rain are usually flagged as bad and eliminated. *Range corrections* also include

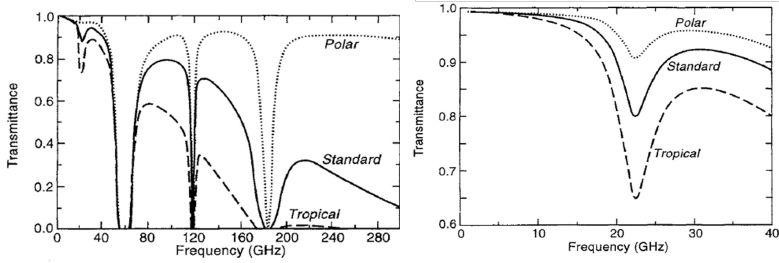


Figure 2.6: Transmittance of subpolar (dotted line), midlatitude (solid line) and tropical (dashed line) cloud-free atmospheres at normal incidence angle as a function of frequency in the microwave band 1-300 GHz. Reproduced from Chelton et al. (2001).

the Sea State Bias effect (ΔR_{SSB}), due to the biased assumption that troughs and crests on the sea surface have the same reflectance and distribution.

- *Geophysical corrections* are actual geophysical signals that are optionally subtracted from the observed SSH in order to make it consistent with the process under investigation. These are the ocean and solid earth tides (Δh_{tides}) and the signal induced by the ocean surface response to variations of atmospheric pressure at low and high frequencies (Dynamic Atmosphere Correction, Δh_{atm}).

Finally, the corrected SSH estimate is related to the observed range R_{obs} as:

$$\begin{aligned}
 SSH &= H - R_{corr} - \Delta h \\
 &= H - (R_{obs} + \Delta R_{dry} + \Delta R_{vap} + \Delta R_{iono} + \Delta R_{SSB}) \\
 &\quad - (\Delta h_{tides} + \Delta h_{atm}) \quad (2.3)
 \end{aligned}$$

More details on the physical processes underlying each correction are reported in appendix (a comprehensive review of theory can be found in Chelton et al. (2001)). Corrections estimates derive either from operational models outputs or from simultaneous measurements taken by instruments on board of the satellite (altimeter and radiometer). Each correction comes from a different source and require specific screening and data flagging. In coastal areas, corrections are often inadequate and traditional screening need to be reimplemented (Andersen and Scharroo, 2011): tides and the response to atmospheric pressure require in these areas much higher resolution models to resolve local rapid changes in the sea level and the complex frictional interaction with land; measurement-derived corrections, such as ionospheric, wet tropospheric and sea state bias are subject to land contamination in the instrument footprint, so require specific procedures for outlier removal and reconstruction (Birol et al., 2017). Improved solutions are investigated within the coastal altimetry community through the above mentioned projects (e.g. PISTACH, COASTALT). Interactive archives such as the RADS³ allow the users to select specific corrective products in order to create the desired SSH dataset. Other projects use dedicated post-processing procedures which improve each correction separately and provide the finite SSH product (e.g. the X-TRACK software, developed at the Laboratoire d'Etudes en Géophysique et Océanographie Spatiale (LEGOS), Roblou et al., 2007, 2011; Birol et al., 2017).

2.2.4 Data dissemination

Measurements from pulse-limited altimeters are generally transmitted by the satellite to the ground at a frequency of 20 Hz along track ($\approx 350m$). Space agencies are then in charge to further process the measurements and complement them with all the required information (flags, corrections, auxiliary variables) before distribution to the end users. The standard along-track products result from further averaging the 20 Hz observations into 1 Hz data ($\approx 7km$), which is the limit frequency allowing detection of mesoscale processes with a significantly high signal to noise ratio.

Based on the processing level, data distributed by space agencies are categorized as:

- **L1:** along-track data processed to the sensor unit and time referenced but not reported on homogeneous space-time grids;
- **L2:** as L1 but geophysical variables at the same locations of observations are included (e.g. geophysical corrections to altimetric range, auxiliary variables

³<http://rads.tudelft.nl/rads/rads.shtml>

like quality flags or external product of MSSH, MDT, geoid heights);

- **L3:** variables regridded on uniform along-track space-time grids, with added completeness and consistency;
- **L4:** model outputs or results from optimal interpolation of lower-level data.

2.3 Satellite altimetry and ocean dynamics

Sea surface height observed by altimetry is referred to an ellipsoidal surface, which is the mathematical reference for the orbit trajectory. SSH encompasses three different signals, in addition to the error ϵ (Fig. 2.1):

$$SSH_{obs} = h_g + \langle \eta \rangle + \eta' + \epsilon \quad (2.4)$$

h_g represent the geoid undulations, which coincide with the geopotential surface closest to the sea level, i. e. with the level of ocean water in a state of rest. This distribution of water masses is induced by the Earth gravitational field. $\langle \eta \rangle$ and η' are respectively the Mean Dynamic Topography (MDT) and the Sea Level Anomaly (SLA). They constitute the mean and the time variable components of the ocean Absolute Dynamic Topography (ADT), which is the dynamical signal of interest for oceanographers (Rio et al., 2004). This displacement with respect to the geoid surface is induced by dynamics of ocean waters on a rotating Earth, forced by the interaction with the atmosphere and lateral and bottom topography. The error ϵ includes instrumental errors as well as the other signals removed by range and geophysical corrections.

For oceanographic purposes, the dynamical component of the altimetric signal must be separated from its geodetic component. This would require in principle to know the geoid field at a resolution and accuracy comparable to those of altimetry. However, the development of geoid models lags behind the advances in altimetric technologies (Bingham et al., 2014). As a consequence, for oceanographic applications of satellite altimetry the time variable component of ADT is used, i.e. the SLA. A mean of sea surface heights (MSSH) is used along with the SSH observations to create SLA, as the MSSH can be given along track with higher accuracy than the geoid. The SLA though expresses only relative changes in the circulation with respect to the mean signal, inducing ambiguous interpretation of altimeter data in regions where the mean flow kinetic energy is comparable with eddy kinetic energy. For instance, the weakening of an anticyclonic pattern could be misinterpreted as a cyclonic signal. An accurate determination of the MDT field is therefore required to

reconstruct the full ADT dynamical signal. This is crucial in many oceanography fields to compute absolute circulation as well as to estimate mass fluxes (Le Grand, 2002). In ocean forecasting a good estimate of MDT is fundamental to better initialize the model, improving prediction skills. In fact, the assimilation of a mean current displaced with respect to reality would push the model toward a state dynamically inconsistent with the turbulence observed by the SLA field.

2.3.1 Methods of Mean Dynamic Topography computation

MDTs have been computed in the past from climatological in situ data (Levitus et al., 2001). They were computed from dynamic height compilations based on hydrological profiles spanning several decades. This solution present some disadvantages such as heights referenced to an arbitrary level of no motion that can miss out part of the surface dynamic topography. Moreover, the spatial data coverage required to reduce the variability noise is obtained with long time series, which cannot be adapted to match specific reference periods.

Other MDT products are derived from long term averages of Ocean General Circulation Models outputs, being though influenced from model biases. Partial correction can be achieved *a posteriori*, for instance through iterative data assimilation (Ezer et al., 1993; Dobricic, 2005).

The ‘direct method’ consist in the difference between a long term time average of altimetric sea surface heights and a geoid model (Menna et al., 2013; Bingham et al., 2014; Woodworth et al., 2015). The direct estimation from altimetry makes the MDT derived with this technique consistent with the SLA observations distributed by space agencies. Moreover it allows to compute full dynamic heights, and consequently absolute surface currents, avoiding to assume an arbitrary level of no motion. Even though MSSH products can resolve details of ocean topography down to 10 km, in this case MDT spatial resolution is limited by state of the art geoid models (Bingham et al., 2014). In Fig 2.7 the raw unfiltered (top panel) and filtered (bottom panel) difference between CLS01 MSSH and the EIGEN-GRGS.RL02 geoid model is shown. It results evident that fine geoid structures are observed by the MSSH but not by the geoid model: large scale filtering ($\approx 1000 \text{ km}$ in this case) is required to remove this noise, that is why at present the direct method cannot be used for regional purposes (Siegismund, 2013). Satellite-only geoid models, as the latest releases of the Gravity field and steady-state Ocean Circulation Explorer mission (GOCE), are highly accurate at long wavelengths, thanks to the global and homogeneous coverage given by the satellite measurements (sub-centimetric accuracy is reached for scales of $\approx 250 \text{ km}$). Regional applications require high resolution

3. Satellite altimetry and ocean dynamics

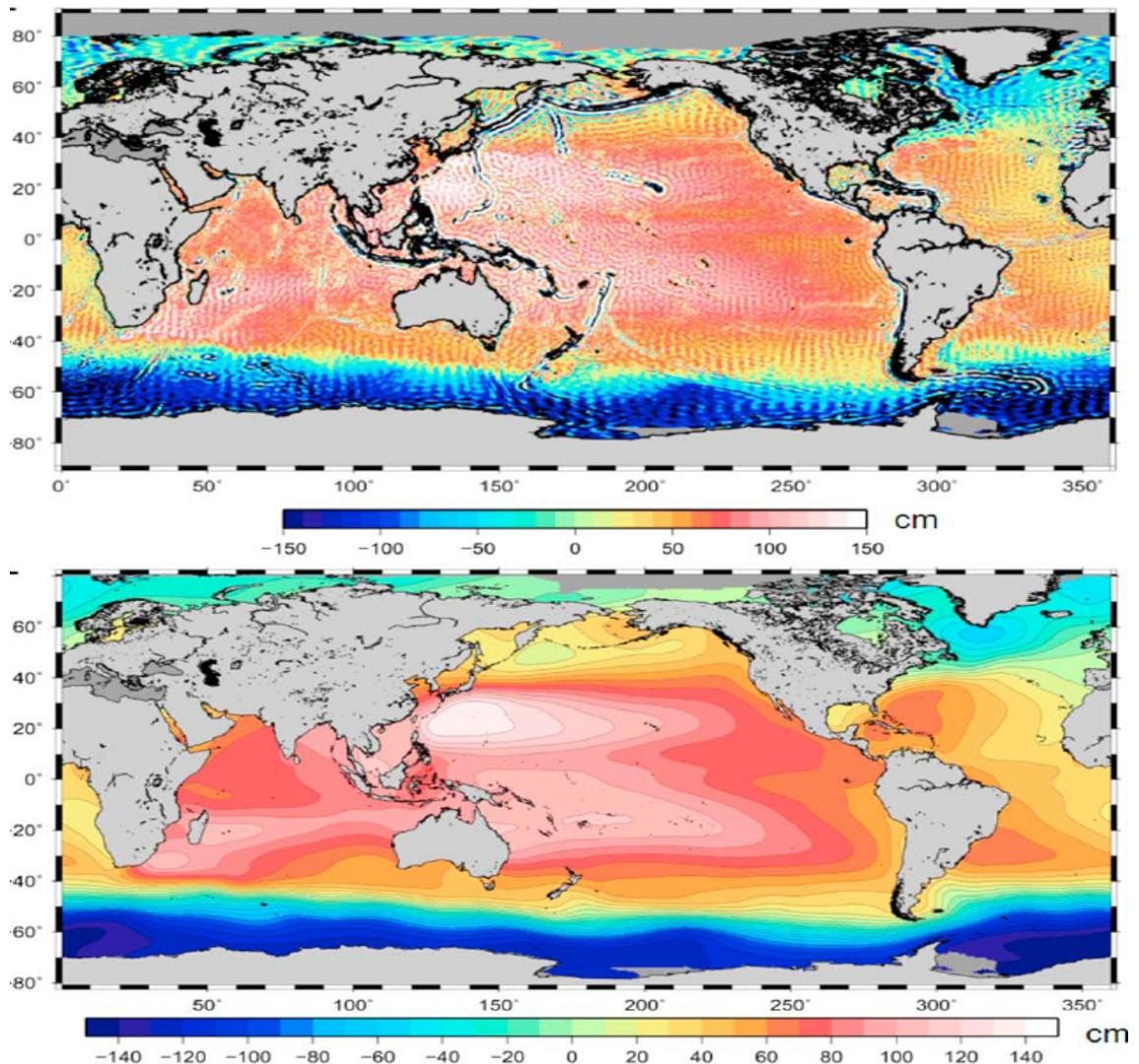


Figure 2.7: Raw unfiltered (top panel) and filtered (bottom panel) difference between CLS01 MSSH and the EIGEN GRGS geoid model. High frequency fluctuations in the top panel . Reproduced from Rio and Hernandez (2011)

geoid models, whose implementation depend on the availability and quality of local terrestrial gravity information for the determination of the high frequencies undulations (Vergos et al., 2001). In some cases geoid composite solutions are adopted. These combine GOCE for the low frequencies and other sources for the higher order harmonics⁴, namely regional gravity data or high resolution models such as the Earth Gravitational Model 2008 (EGM2008) (Woodworth et al., 2015; Knudsen and Andersen, 2013; Ophaug et al., 2015). The Mediterranean sea typically require high resolution, since the presence of numerous islands, peninsulae and jagged coastlines reflects steep variations of the geoid in the transitions from land to ocean (Woodworth et al., 2015).

High resolution MDTs are obtained from combinations of the above methods. Optimal interpolation is used to integrate a first guess and in situ oceanographic data. The former ensures data homogeneity throughout the considered basin, depicting the basin scale circulation patterns, while the latter defines the fine scales.

For global MDTs, a low resolution first guess derived with the direct method is enough to represent synoptic circulation patterns. In Rio and Hernandez (2011) the filtered MDT shown in Fig 2.7 is refined using independent in situ measurements and altimetric data to obtain the CNES–CLS09 MDT for the world ocean on a 1/4 of a degree resolution grid.

Due to a complex topography and the mid-latitude position, few MDTs have been evaluated in the Mediterranean sea by the direct method (Menna et al., 2013; Woodworth et al., 2015). However, these products are not distributed to the public since these studies are just at an early stage. At present only models can give a high resolution basin wide representation of the sea level in this sea. The SMDT-MED-2014 computed by Rio et al. (2014) for the Mediterranean sea is a high resolution MDT (1/8 of a degree). It is based on a first guess derived from a long term average of the reanalysis produced from the MFS forecast (Adani et al., 2011). An iterative procedure improves the first guess with in situ ‘synthetic’ estimates derived from drifter velocities and hydrological profiles.

The lack of an accurate MDT derived with direct method in the Mediterranean Sea encourages our study for such product.

⁴<http://www.goco.eu/>

Chapter 3

Sea Surface Height signal analysis

In this work, a Sea Surface Height dataset along Jason 2 satellite (hereafter J2) tracks is created as intermediate step to obtain a Mediterranean Sea MDT throughout a 'direct method'. The present chapter describes the processing applied for the creation of this dataset (hereafter R-SSH) and the computation of Mean Sea Surface Height along track profiles (hereafter R-MSSH) and the Sea Level Anomalies relative to them (R-SLA). The R-SLA are compared in this chapter to the TAPAS SLA operational dataset used by MFS, in order to validate the ALES dataset and to quantify the coverage gained in coastal areas (for reference details about TAPAS dataset see subsection 1.2.3). The R-MSSH are used to derive the along track MDT for the Mediterranean, as described in chapter 4.

3.1 Data processing

Data used to create the R-SSH are Coastal Geophysical Data Records (CGDR) from the Ocean Surface Topography Mission (OSTM, Dumont et al. (2016)) on board of J2. The altimetric parameters of the CGDR have been recently retracked by the UK National Oceanography Centre with the ALES coast dedicated algorithm (Adaptive Leading Edge Subwaveform retracker, Passaro et al., 2014; Cipollini et al., 2015). This algorithm analyses iteratively single altimetric waveforms in order to detect the positions of spurious peaks and consequently adapt the retracking window (see Fig 2.5a in subsection 2.2.2). ALES dataset is packaged in L2 processing level data files by the British Oceanographic Data Centre, and distributed by the Physical Oceanography Distributed Active Archive Center (PODAAC, files available via ftp at ftp://podaac.jpl.nasa.gov/allData/coastal_alt/L2/ALES/). Data along thirty J2 tracks covering the Mediterranean sea in the period from July 2008 (cycle 1) to May 2015 (cycle 252) are used in this work. Ground tracks are shown in 3.1,

the spatial separation between tracks is approximately 200 km and the orbit repeat period is 10 days.

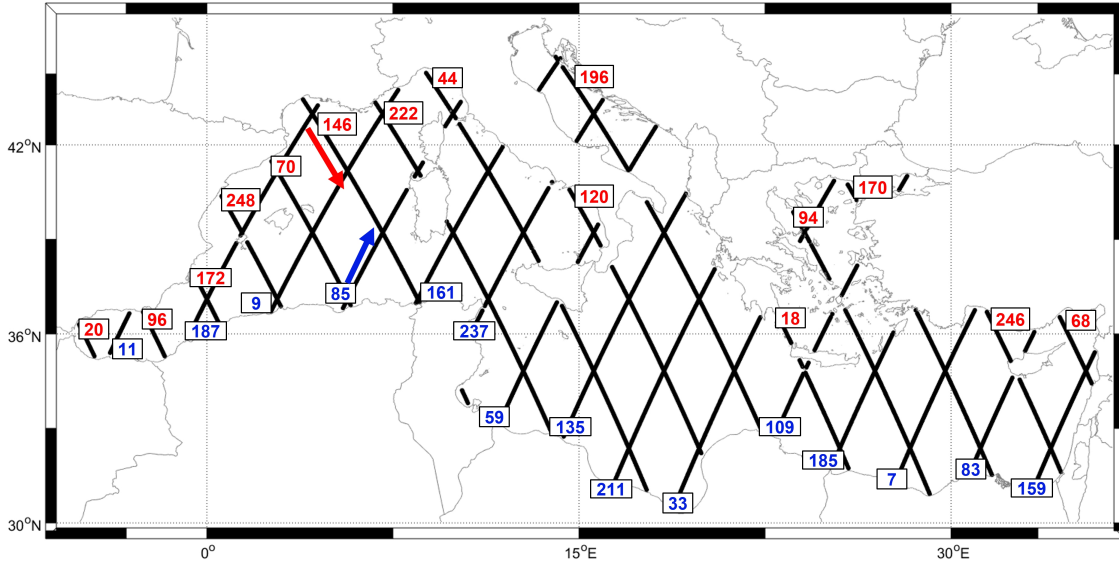


Figure 3.1: Portion of J2 30 tracks over the Mediterranean used to compute R-SSH; ascending tracks are color coded in blue while descending in red.

3.1.1 Pre-processing

ALES algorithm is applied to the single altimeter waveforms as transmitted by the satellite to the ground, and is distributed at the original frequency (20 Hz), without further processing (Cipollini et al., 2015). Hence some pre-processing operations are required to turn the retracked range into an useful oceanographic signal:

- ALES *range* values are selected based on the waveform fit error provided in the CGDR data files: estimations having fitting error of over 0.5 are excluded, as suggested in Passaro et al. (2015);
- The 20 Hz ALES measurements are smoothed along track using a 21 points wide moving average, shaped by gaussian weights based on the distance from the central point of the average window;
- 20 Hz SSH are computed using the smoothed ALES range together with orbit and corrections ($SSH = orbit - (range + corrections)$);
- SSH estimates are excluded if their value deviated more than 3 meters or 3 median absolute deviations (MAD) from the median value within the 21 points

1. Data processing

moving window. MAD is defined as:

$$\text{MAD} = \text{median}(|X - \text{median}(X)|) \quad (3.1)$$

where X is the vector containing the 21 points (following Passaro et al. (2015)).

The corrections used are listed below (solution adopted are reported in J2 handbook, Dumont et al. (2016)):

- **Dry troposphere correction** (file variable named *model_dry_tropo_corr*): the effect of dry gases is proportional to the Sea Level Pressure (SLP). SLP is given by the along track interpolation of European Centre for Medium-Range Weather Forecast (ECMWF) meteorological fields;
- **Wet troposphere correction** (file variable named *rad_wet_tropo_corr*): derived from measurements of brightness temperatures made by the on board Advanced Microwave Radiometer; the solution adopted here is computed with an algorithm which adapts to the interpretation of both pure ocean and mixed land/ocean scenes (Brown, 2010); flagging rain events is not straightforward. Despite techniques to identify rain events have been suggested (Tournandré and Morland, 1997), existing algorithms in some cases miss the detection or falsely discard good data. Rain flags are at present not well implemented in J2 Geophysical Data Record products (Thithonis and Achuthan, 2013). J2 data records include two rain flags: one based on radiometer measurements and another based both on radiometer and dual-frequency altimeter measurements. As the latter removes a portion of coastal measurements with a suspiciously homogeneous pattern, which would constitute a limitation in our case, the former flag has been chosen;
- **Ionospheric correction** (file variable named *iono_corr_gim_ku*): the effect of Ionosphere on the radar pulse is proportional to its Total Electron Content (TEC). Maps of TEC for the corrections used in this work are developed by the Jet Propulsion Laboratory of National Aeronautics and Space Administration (JPL-NASA). An alternative correction based on dual-frequency altimeter measurements is not taken in consideration because spikes due to the presence of land degraded the quality of coastal data;
- **Sea state bias correction** (file variable named *sea_state_bias_ku*): SSB estimates are determined from a look up table based on SWH and backscatter coefficient (σ_0). Using SWH and σ_0 retracked with ALES as references would

be the optimal solution, with the drawback of adding further uncertainty to our results. Hence the standard SSB values are used in this work;

- **Tidal correction**

(file variables named *solid_earth_tide*, *pole_tide*, *ocean_tide_sol1*): solid earth tide is calculated as the solid earth radial response to tidal potential computed by Cartwright and Tayler (1971) and Cartwright and Edden (1973); pole tide is the response of solid earth and oceans to centrifugal potential caused by small perturbations in Earth's rotation axis (computed by Wahr (1985) and adapted to the current era); ocean tides are given by along track interpolation of the main harmonics as predicted by GOTv4.8 model (by NASA's Goddard Space Flight Center).

The **Dynamic Atmosphere Correction (DAC)**, related to the effect of atmospheric pressure, is not applied since this forcing is at present already modelled in MFS system (Dobricic et al., 2012). This feature was introduced in MFS because the semi-enclosed nature of the Mediterranean Sea is responsible for complex responses of the ocean surface to atmospheric pressure which are not properly reproduced by the DAC correction (Candela and Lozano, 1994). Consistently, the TAPAS datasets is also used without DAC correction.

In Fig 3.2 is shown an example of along track SSH before and after pre-processing for the track 120, cycle 118 (September 2011).

3.1.2 Target grid definition and 1 Hz averaging

J2 satellite uses a repeat orbit and flies over the same ground track each 10 days. However, the satellite orbit is not completely controlled and the position of measurements at ground is subject to small cross track and along track shifts (magnitude 1-2 km). Thus, measurements are not made at the exact same locations over the cycles and a co-location process on a target track grid is necessary in order to build up homogeneous time series and evaluate the R-MSSH time average.

A target grid at 1 Hz is created taking as reference the CLS 1-Hz track used for the TAPAS SLA product. Histogram in Fig 3.3 shows the number of points of the target grid as function of radial distance from the coast. The distribution peaks between 20 and 40 km, due to the presence of many island all over the Mediterranean Sea. This shows that most of the satellite measurements in the Mediterranean sea are taken in coastal areas.

1. Data processing

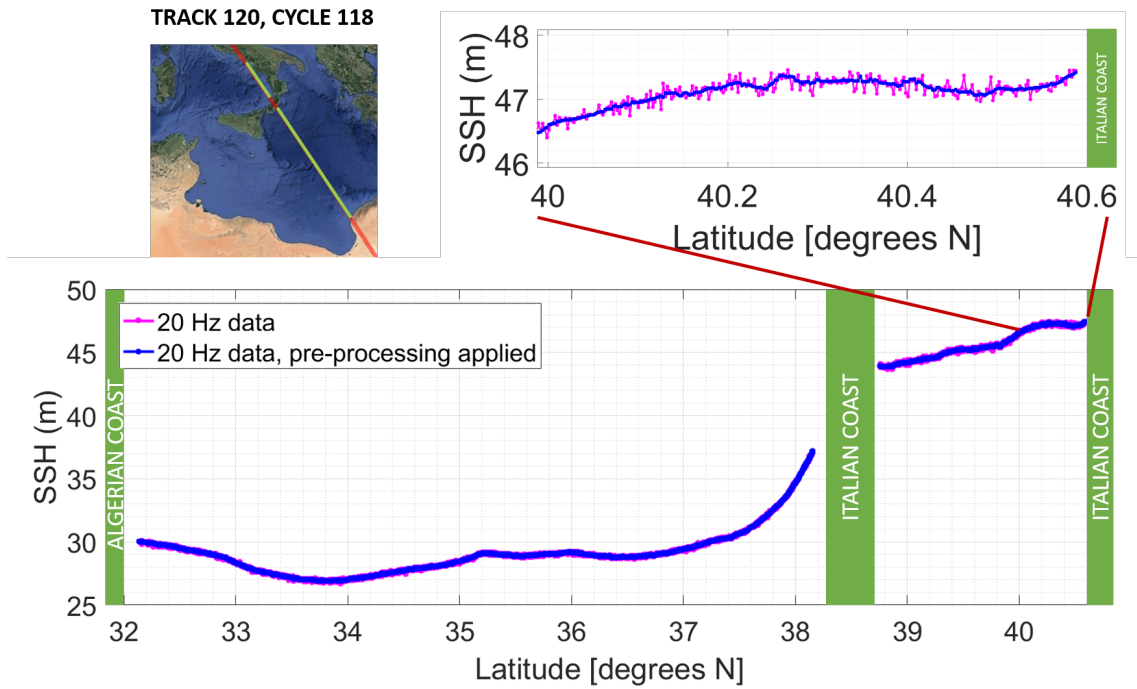


Figure 3.2: SSH values along J2 track number 120 and cycle 118 valid during September 2011. Before (pink line) and after (blue line) pre-processing.

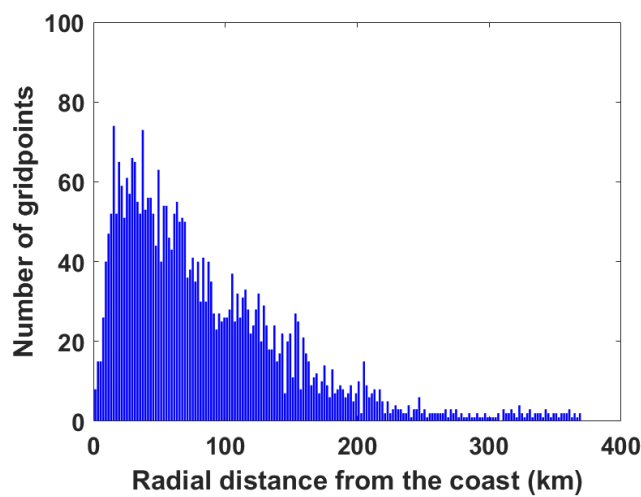


Figure 3.3: Distribution of target grid points as function of radial distance from the coast.

The co-location process is performed in order to extrapolate SSH values on the target grid because the observed ground tracks are cross-track and along-track shifted. The best extrapolation can be reached only with a perfect estimate of the Cross Track Geoid Gradient (CTGG). Since CTGG is difficult to be distinguished from the gradient induced by the ocean dynamics (Dibarboure et al., 2012), we preferred to compute SSH at 1 Hz target grid points as the average of 20 Hz measurements within a research radius of 3.5 km, as shown in Fig 3.4.

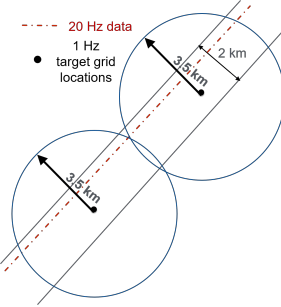


Figure 3.4: Method for co-location of ALES 20 Hz data at target grid locations: 20 Hz measurements (red dotted line) within 3.5 km from each point of the target grid (black dot) were averaged to compute 1 Hz SSH estimates.

Time series resulting from the co-location process cover the period from July 2008 to May 2015; this dataset will be referred hereafter and in the following chapters as R-SSH. Values in time series further than 4 standard deviation from the time average are considered outliers and excluded from the analysis. Mean values of R-SSH (hereafter R-MSSH) are computed at each target grid location and subtracted from R-SSH to obtain a set of 1 Hz anomalies (hereafter indicated as R-SLA).

3.2 Comparison with the operational Sea Level Anomaly dataset

In this section we want to assess the feasibility of retracked ALES data to increase the number of SLA observations near the coast with respect to the actual operational database TAPAS. The two datasets will be initially compared at their respective original resolution (prior co-location of ALES data). This first assessment will look at how further the ALES dataset approaches the coast with respect to TAPAS along J2 tracks. Then, R-SLA time series, obtained after the co-location, will be compared to those of TAPAS SLA in terms of continuity (no data gaps) and homogeneity (no outliers) in coastal areas.

3.2.1 Comparison of SLA datasets at original resolution

Given that ALES original resolution is 20 Hz (≈ 350 m, see subsection 3.1.1), while TAPAS resolution is 1 Hz (≈ 7 km, see subsection 2.2.4), a first qualitative comparison was estimated as the information gain of the two datasets given by their Closest Point of the ground tracks to the coastline, called CP. We could compare the datasets over 54 comparison points (red points on each side of the blue delineated tracks in Fig 3.5a). Fig 3.5b shows the average distance of CPs during the 252 cycles of the tracks for each dataset. We can see that ALES retrieves information up to a couple of kilometres (for example along the eastern Adriatic coast, see sites number 12,14,17,18). Moreover, STD of ALES dataset is lower compared to TAPAS, meaning that, for the former, closer CP positions are often observed (see Fig 3.5c). TAPAS CP never overcomes ALES CP, and on average TAPAS CP is at a distance of 10 km, with some extreme cases of 30 km from the coasts (see sites number 11, 13, 21). At almost all sites the difference between CPs of the two datasets ranges from 5 to 30 km. Potentially ALES can add from one to four 1 Hz resolution observations.

3.2.2 Comparison of SLA datasets on target grid

In this section we compare R-SLA values, obtained from ALES dataset after colocation on the 1 Hz target grid, to TAPAS SLA dataset on the same grid. Since SLA TAPAS are available starting from cycle number 211 (March 2014), the comparison is carried out over a limited 1-year period (2014-2015). Examples of the R-SLA and SLA TAPAS time series in three areas are shown in Figg 3.6 (Gulf of Lion), 3.7 (Gulf of Taranto) and 3.8 (southern coast of Turkey); for each area an offshore and a coastal grid point are displayed, and reference areas are encircled in Fig 3.9b. Offshore time series of the two datasets (top panels of the three figures), have similar amounts of data and high correlation. Close to the coast (bottom panels) the TAPAS time series show a reduced number of estimates. We can also notice an increased offset between the two datasets from west to east, which reach 10 cm at site C (Fig 3.8). This might be explained by the fact that no correction for Long Wave Errors have been applied to the R-SLA dataset, while this effect is corrected in TAPAS dataset as described in Le Traon et al. (1998). It must be also noticed that mean sea surface heights used to compute the two dataset are referenced to different periods (2008-2015 for the R-SLA and 1993-2012 for TAPAS SLA). Hence interannual and decadal variability may determine the observed differences.

In Fig 3.9 is shown the percentage of valid cycles (when the observation was not

2. Comparison with the operational Sea Level Anomaly dataset

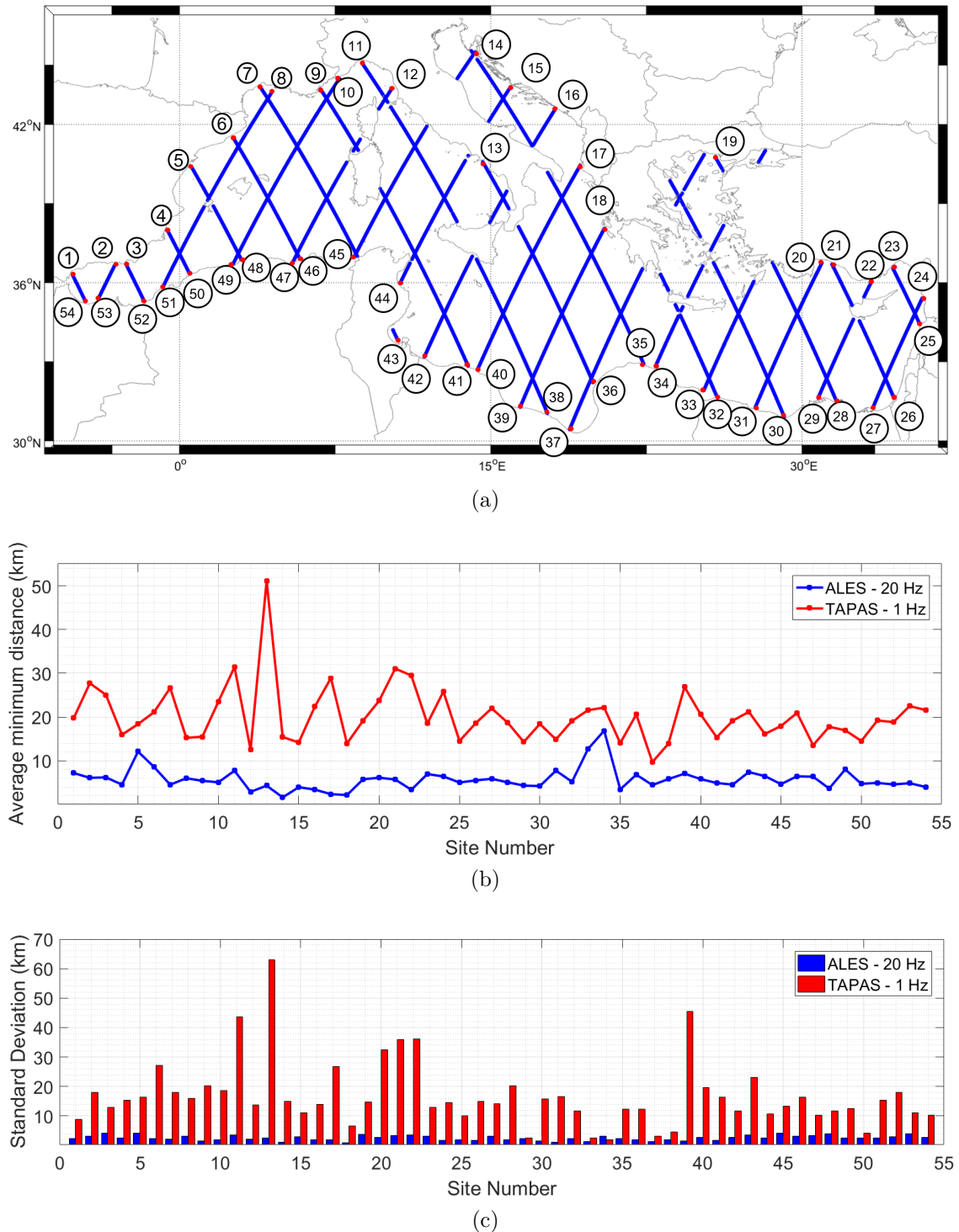


Figure 3.5: Comparison of ALES and TAPAS datasets distance to the coast: (a) reference points chosen for the comparison along the Mediterranean coasts (red dots, J2 tracks are reported in blue as reference); (b) time averaged distances of ALES (blue) and TAPAS (red) at the reference points indicated in Fig 3.5a; (c) As in (b) but for standard deviations.

2. Comparison with the operational Sea Level Anomaly dataset

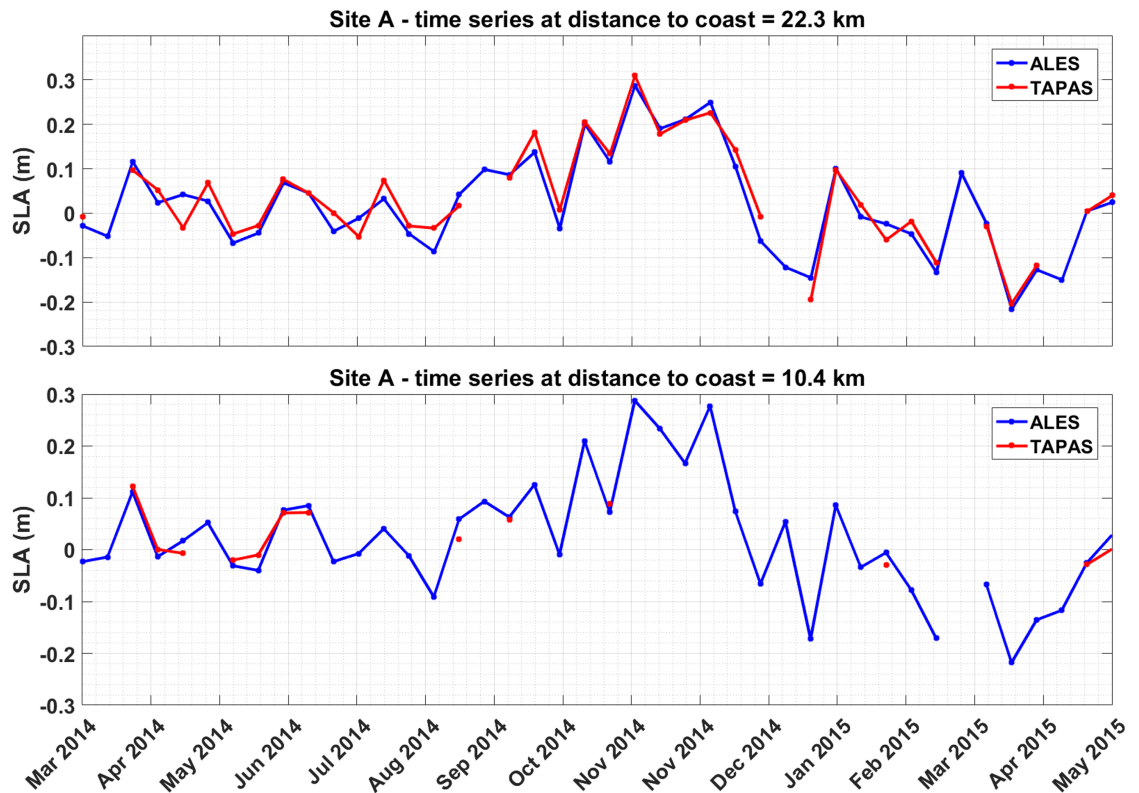


Figure 3.6: Comparison of ALES-derived R-SLA (blue) and TAPAS SLA (red) time series in the area of the Lion Gulf (position is reported in Fig 3.9b). Time series for an offshore gridpoint are displayed in the top panel while for a coastal gridpoint in the bottom panel.

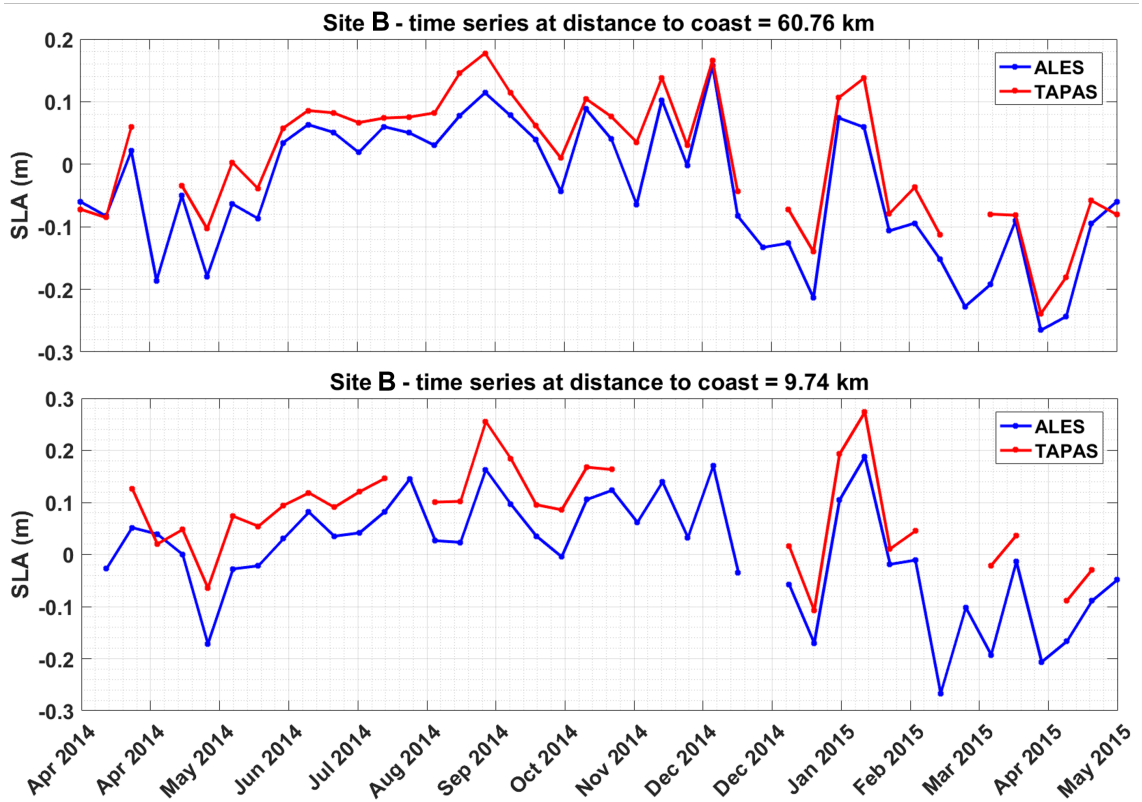


Figure 3.7: Comparison of ALES-derived R-SLA (blue) and TAPAS SLA (red) time series in the area of the Taranto Gulf (position is reported in Fig 3.9b). Time series for an offshore gridpoint are displayed in the top panel while for a coastal gridpoint in the bottom panel.

2. Comparison with the operational Sea Level Anomaly dataset

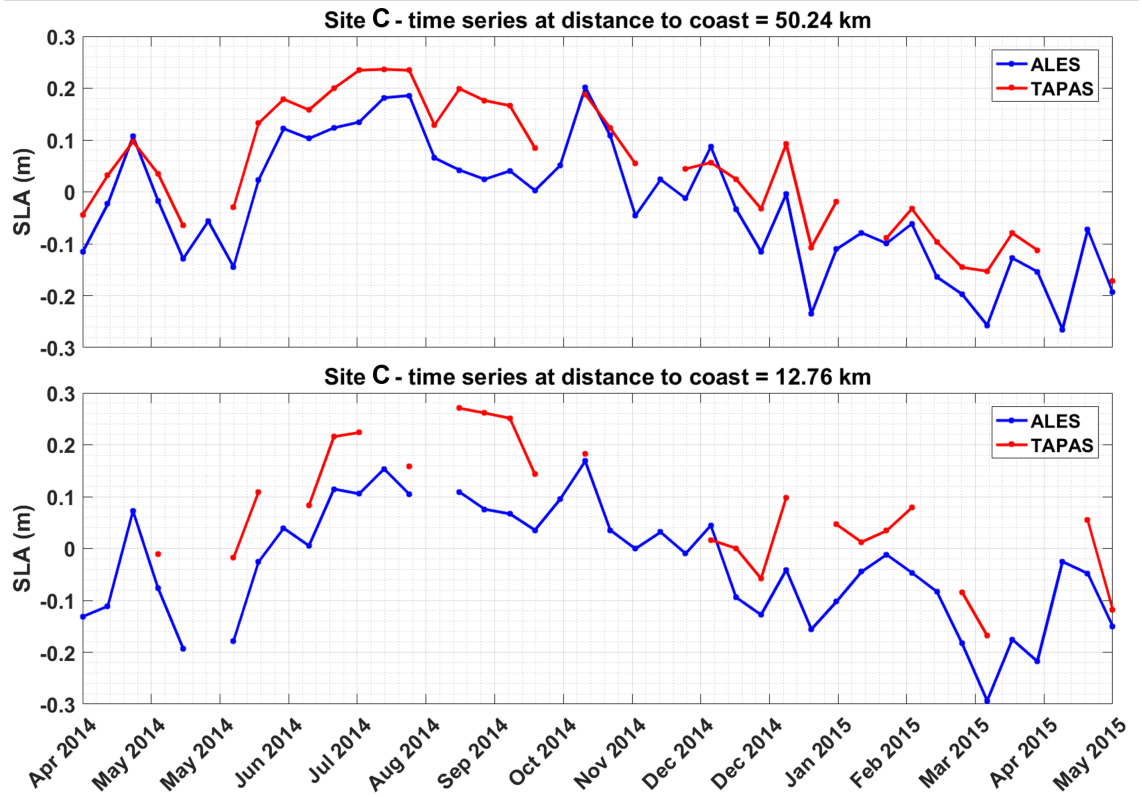


Figure 3.8: Comparison of ALES-derived R-SLA (blue) and TAPAS SLA (red) time series along the southern Turkish coast (position is reported in Fig 3.9b). Time series for an offshore gridpoint are displayed in the top panel while for a coastal gridpoint in the bottom panel.

2. Comparison with the operational Sea Level Anomaly dataset

considered outlier) at each target grid point for the two datasets. We notice that globally R-SLA has a higher number of available cycles with respect to TAPAS SLA, and this difference is enhanced in coastal areas. While ALES dataset has more than 80% of cycles almost everywhere, TAPAS goes down to 60-50% in some areas like the Alboran sea, the southern Italian coasts and in the Aegean sea.

In Fig 3.10 is displayed the along track Standard Mean Error (SME) of the two datasets, defined as the standard deviation σ normalized by the number of valid cycles N at the grid point j :

$$\text{SME}_j = \frac{\sigma_j}{N_j} \quad (3.2)$$

The spatial distribution and magnitude of SME for the R-SLA are consistent with those of TAPAS SLA. R-SLA well reproduces the high variability in the Alboran and Algerian seas and in the Ionian and Levantine basins (Pascual et al., 2007). Reasonable values of SME are observed also in coastal regions where R-SLA has a larger percentage of cycles with respect to TAPAS (Alboran sea, the southern Italian coasts and in the Aegean sea). In these areas, despite the signal being potentially corrupted by the presence of land, ALES is able to reconstruct robust time series and recover useful information by retracking.

2. Comparison with the operational Sea Level Anomaly dataset

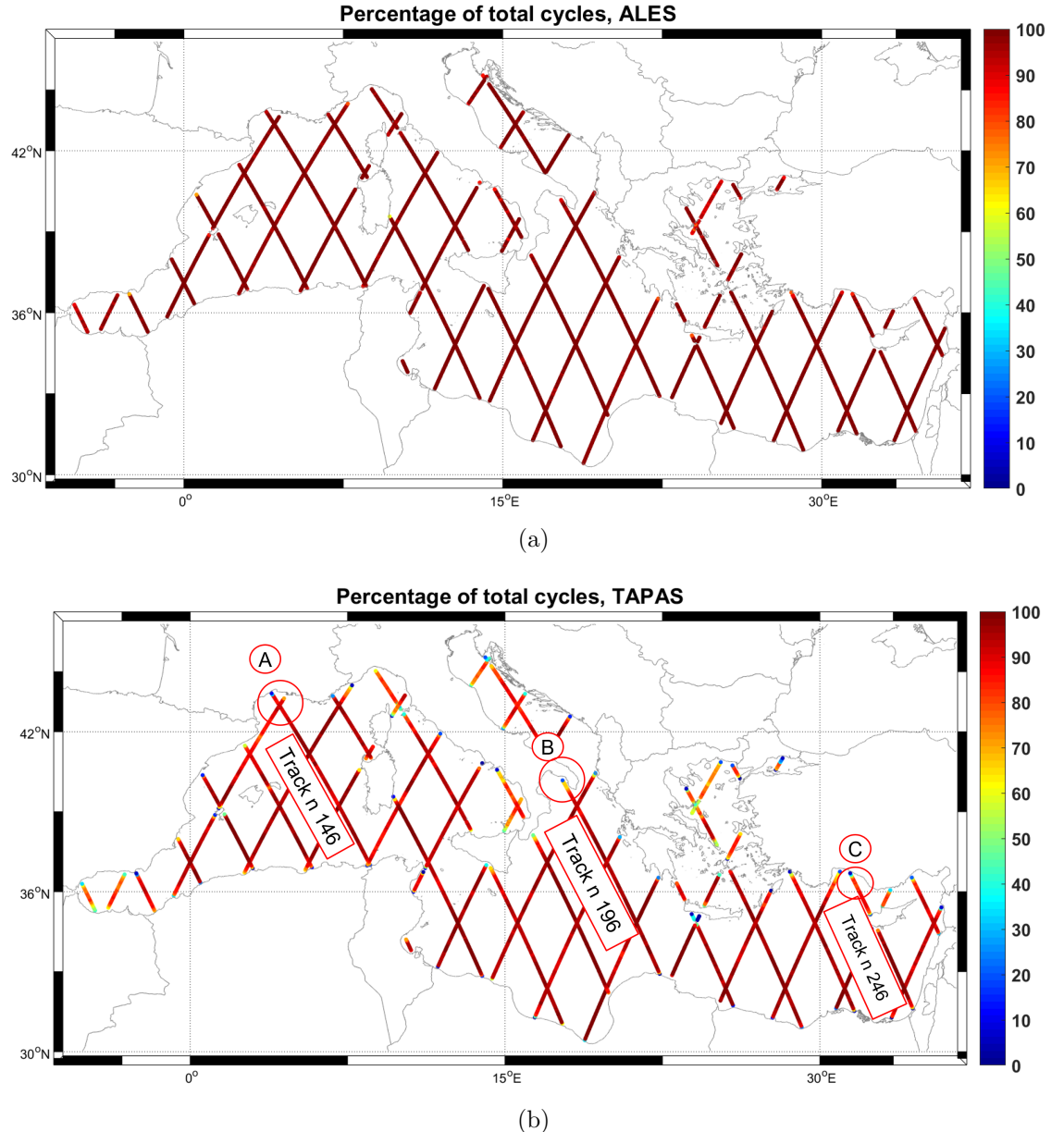


Figure 3.9: Percentage of valid cycles at each grid point for R-SLA (a) and TAPAS SLA (b) datasets; percentages are relative to the total number of cycles between March 2014 and May 2015. Areas encircled in (b) are indicated as reference for the time series of R-SLA and TAPAS SLA shown in Figg 3.6, 3.7, 3.8.

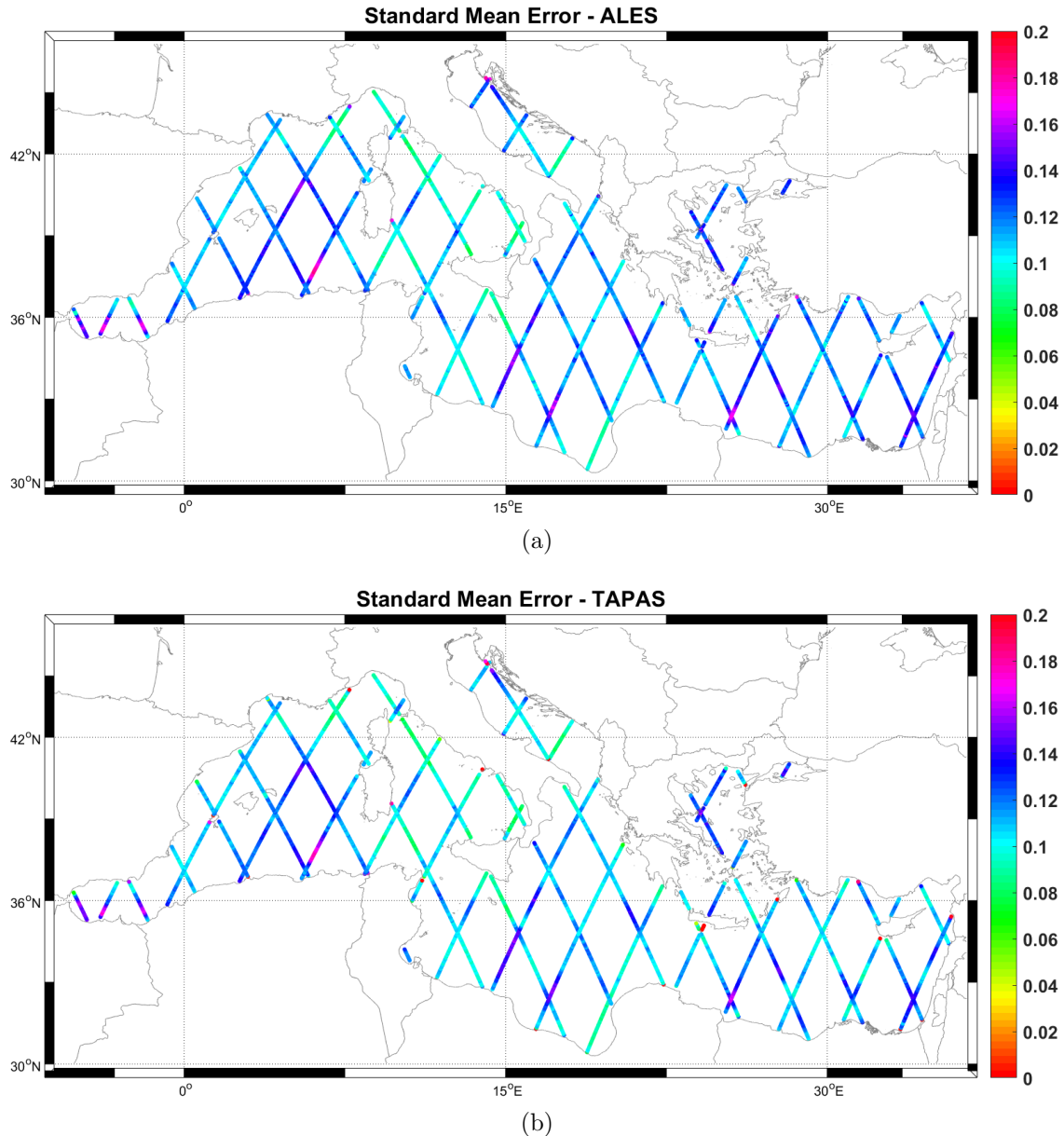


Figure 3.10: Along track Standard Mean Error for the R-SLA (a) and TAPAS SLA (b) datasets. Values for the two datasets show consistency.

Chapter 4

Mean Dynamic Topography computation and evaluation

The final objective of this work is the computation of a MDT for the Mediterranean Sea through the direct method, previously described in subsection 2.3.1. Methods and results are presented in this chapter, including a depiction of the main circulation patterns and a comparison with the SMDT-MED-2014 product by Rio et al. (2014). Discussion of results will follow.

4.1 Data and Methods

In this part we make use of the mean sea surface height R-MSSH computed along the Jason 2 (hereafter J2) tracks from ALES dataset as described in subsection 3.1.2 and of the EGM2008 geoid model. Since the R-MSSH is computed based on observations covering the years 2008 to 2015, the MDT computed here is referred to that period. One should be careful in the comparison with the SMDT-MED-2014, which is instead referenced to the period 1993-2012. The EGM2008 undulations, gridded on a 2.5×2.5 minutes of degree, is available on the National Geospatial intelligence Agency (NGA) website¹. EGM2008 model was chosen for this work because of its high spatial resolution (coefficients estimation complete to do 2159, nominal resolution of about 10 km), which makes its performance comparable with contemporary detailed regional geoid models (Pavlis et al., 2012). Even though composite geoid models are the best option in terms of accuracy both at high and low frequencies, there are no official products available, hence their usage was considered beyond the scope of this work. The high frequencies of EGM2008 model are obtained using altimetry, through an iterative procedure which derives free-air gravity anomalies

¹http://earth-info.nga.mil/GandG/wgs84/gravitymod/egm2008/egm08_wgs84.html

from the altimetric signal. The slope of sea surface is hence partially retained in EGM2008, resulting in geoid coastal slopes smoother than the actual gradients in case of steep shelves. This may be an issue for the determination the ocean dynamic topography through the direct method, as is shown in the following analysis.

The first step is the computation of along track estimates of MDT. The EGM2008 is interpolated at the along track target grid locations using a specific routine provided by NGA; geoid heights are referenced to the same ellipsoid used by J2 altimetric mission. Along-track MDT (hereafter R-MDT) is obtained subtracting along-track geoid heights from R-MSSH. R-MDT is shown in Fig 4.1

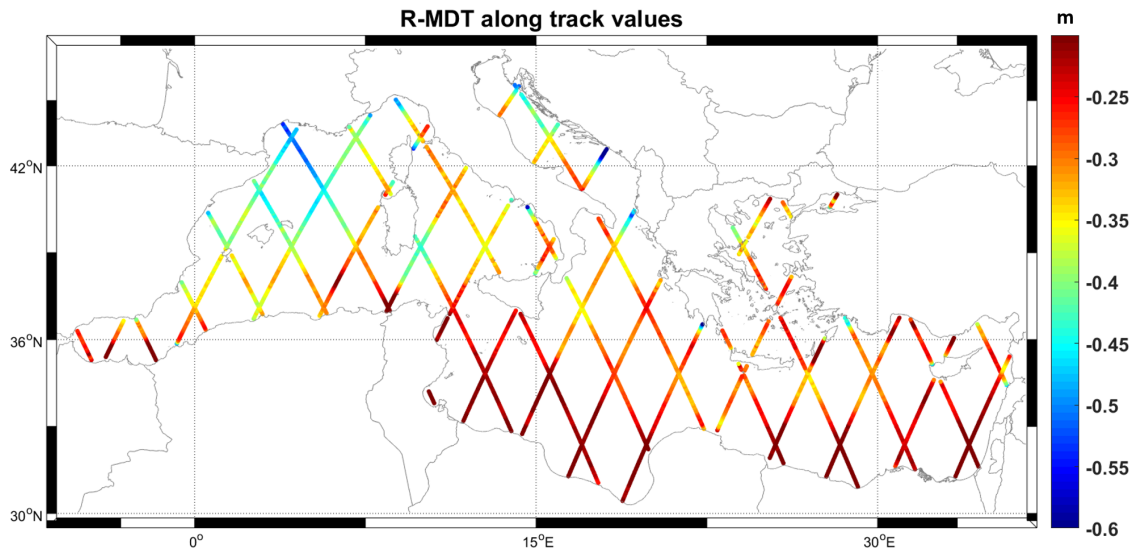


Figure 4.1: Map of along track values of R-MDT derived from ALES altimetric dataset and EGM2008 geoid model. The color scale is reported here to the range [-0.6:-0.2] m.

The second step is the interpolation of the R-MDT observations over the whole basin. Objective Analysis (OA) described in Pinardi et al. (2016) is used to map the R-MDT on a regular grid derived from the MFS model grid. OA parameters define the area of influence of a single observation on the grid, i.e. the degree of smoothing of R-MDT data. In this phase, different grid resolutions and OA parameters are tested in order to propagate the observations over the entire grid with an OA percentage error smaller than 50%. Since the distance between J2 tracks is about 200 km, interpolation is performed using a decorrelation length of 250 km. A regular horizontal grid of 1/4 of a degree resolution is chosen. MDT-ALES map obtained is shown in Fig 4.4a.

In Fig 4.2 the R-MDT for track 146 and SMDT-MED-2014 interpolated along the same track are displayed. We can note here an offset value of about 30 cm. The offset is observed over the entire Mediterranean, and the difference between the

1. Data and Methods

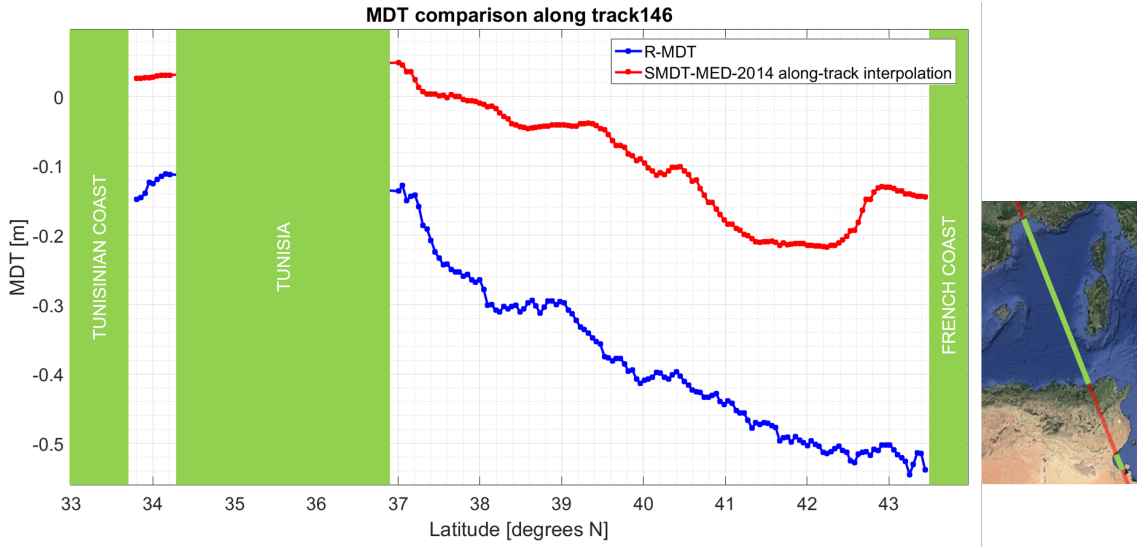


Figure 4.2: Comparison of R-MDT and SMDT-MED-2014 interpolated along track 146 from the Tunisian to the Provencal coasts. An offset of approximately 30 cm is visible; the cyclonic minimum of MDT represented in the SMDT-MED-2014 is not visible in R-MDT.

basin mean of the two MDT is

$$\Delta \overline{MDT} = \overline{SMDT-MED-2014} - \overline{R-MDT} \approx (-0.023) m - (-0.296) m \approx 0.272 m$$

For the basin wide comparison, the difference between the two maps is computed as

$$MDT-ALES - SMDT-MED-2014 + \Delta \overline{MDT}$$

. Hence differences between the two maps will be evaluated in terms of relative patterns.

A map of currents is also derived from the MDT-ALES map assuming that geostrophy is valid at mesoscale and synoptic scale (i.e. spatial scales bigger than some tenth of kilometres and time scales longer than few days). At each grid point j having valid surrounding estimates of MDT (i.e. not Nan values), velocity is computed as:

$$\begin{cases} U_j = -\frac{g}{f_0 \cdot R_E} \frac{\Delta MDT_{j-1,j+1}}{\Delta \phi_{j-1,j+1}} \\ V_j = \frac{g}{f_0 \cdot R_E \cdot \cos(\phi_j)} \frac{\Delta MDT_{j-1,j+1}}{\Delta \lambda_{j-1,j+1}} \end{cases} \quad (4.1)$$

where ϕ is the latitude, λ the longitude, $R_E \approx 6371$ km is the radius of the Earth and the Coriolis parameter is taken constant given the beta plane approximation $f = f_0 + \beta \cdot dy$ where the beta term can be considered negligible; the derivatives are centred at the computation grid point. Velocities VEL-ALES are displayed in

Fig 4.7.

4.2 MDT features and geostrophic velocities

Raw along track R-MDT estimates are presented in Fig 4.1. These are characterized by high frequency fluctuations superimposed on a large scale pattern. Fluctuations, clearly visible in Fig 4.2, have spatial scale of 10-20 km and amplitude of about 5 cm. R-MDT values range between -0.762 m and 0.033 m, with a negative basin mean of -0.296 m. The lowest values are found near the Provencal coast, and in the Adriatic sea, along the Dalmatian coast. The Alboran and Algerian basins, the southern part of the Ionian and most of the Levantine basin are characterized by values higher than -0.25 m. Absolute values of R-MDT differences between tracks at *crossovers* are shown in Fig 4.3. Most differences are ≤ 2 cm, with some values up to 4 cm, which represents approximately 10% of the MDT signal. These values can be taken as an indication of the internal consistency of the R-MDT calculation.

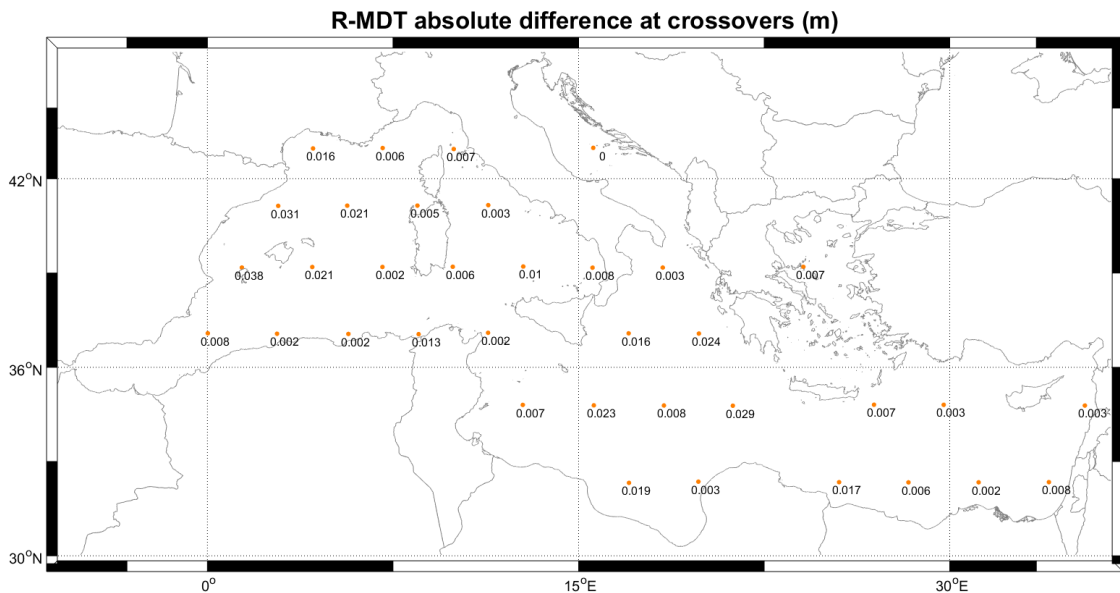


Figure 4.3: Absolute differences of R-MDT values at crossover between different tracks.

Below, the MDT-ALES (Fig 4.4a) and its OA percentage error (Fig 4.4b), the SMDT-MED-2014 (Fig 4.5a) and the difference between the two MDT maps (Fig 4.5b) are shown. In Fig 4.4a, areas with OA percentage error greater than 50% were masked. A general depiction of the basin wide characteristic of MDT-ALES and of the differences with SMDT-MED-2014 follows.

The meridional gradient observed in MDT-ALES is due to the wind forcing, that creates a double gyre structure extending all through the basin. This is formed by

2. MDT features and geostrophic velocities

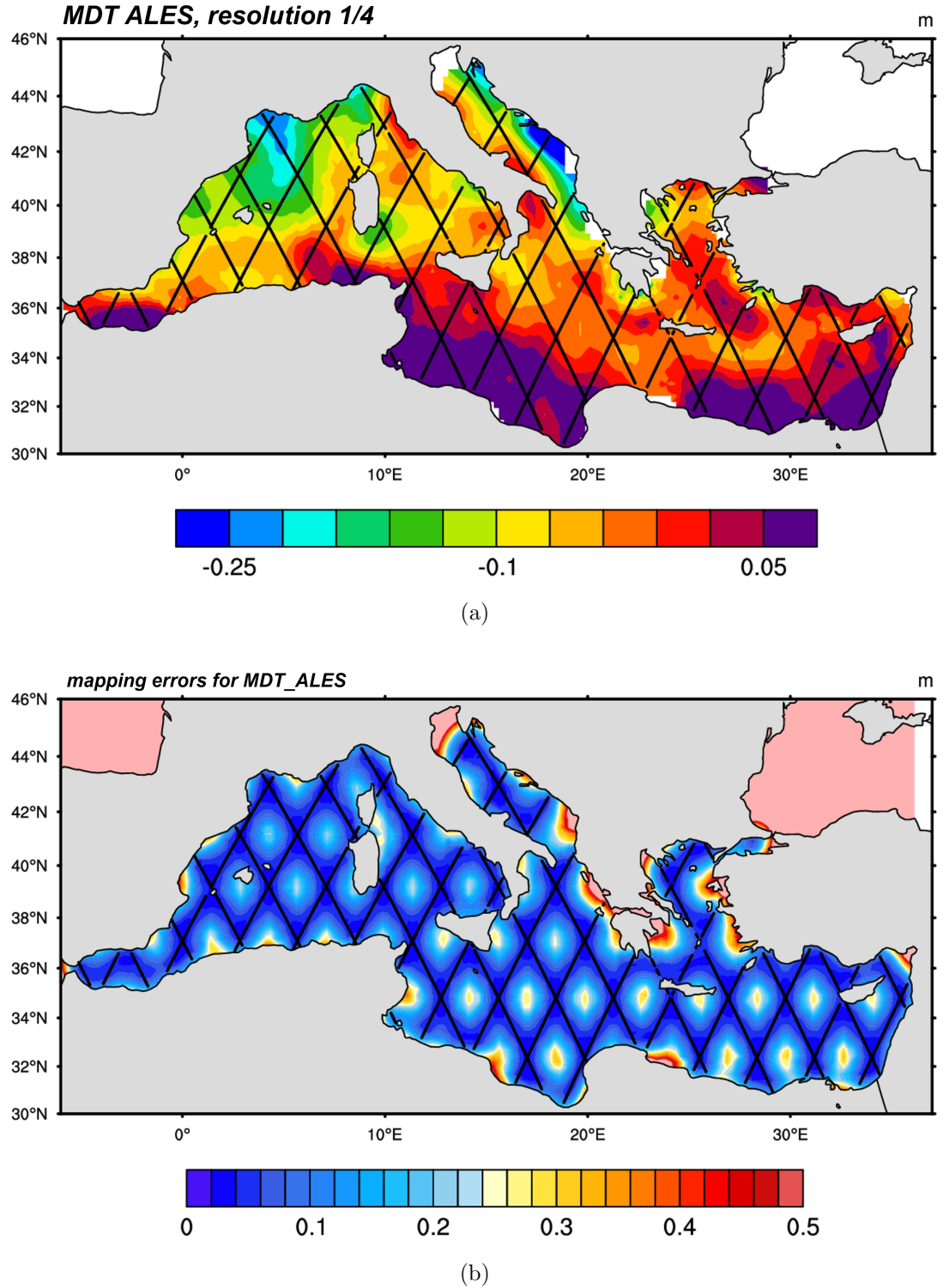


Figure 4.4: MDT ALES map (a) and relative mapping errors (b). MDT-ALES is obtained from optimal interpolation of R-MDT on a regular horizontal grid of 1/4 of a degree resolution (J2 tracks are reported as reference). Mapping error grows with distance from the tracks and maximum values are found at the centre of tracks diamonds and in coastal areas, especially along the Aegean and Adriatic Coasts. Values of MDT with error over 50% are masked.

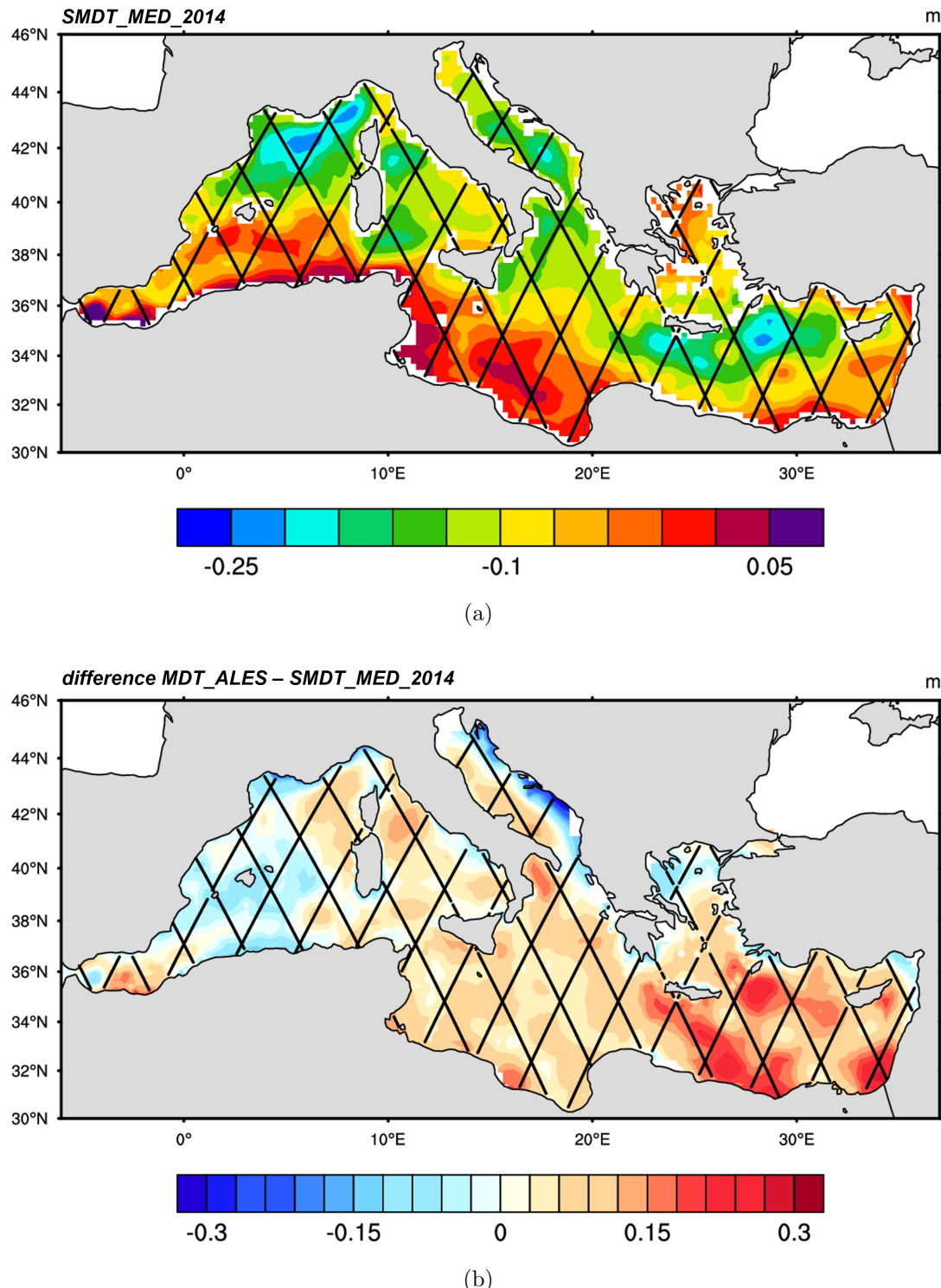


Figure 4.5: (a) SMDT-MED-2014 reported on a regular horizontal grid of 1/4 of a degree resolution. (b) Difference between MDT-ALES (Fig 4.4a) and SMDT-MED-2014.

2. MDT features and geostrophic velocities

cyclonic circulation in the northern Liguro-Provencal sub basin, anticyclones in the southern Ionian basin, delimited by a central eastward cross-basin current, and a cyclonic circulation in the centre of the Levantine sub-basin (Pinardi and Masetti, 2000; Menna et al., 2013). The overall gradient is more intense in the MDT-ALES than in the SMDT-MED-2014. Differences between MDT-ALES and SMDT-MED-2014 (Fig 4.5b) have a longitudinal gradient at the basin scale. With respect to this tendency, enhanced differences are observed along the Adriatic coast and in the western Aegean basin. The same observation is reported also by Woodworth et al. (2015) in a similar comparison between model-derived and altimetry-derived (using geoid EGM2008) MDT maps. The highest spatial variability in the difference between the two MDTs is found in the Alboran and Levantine basins.

Some patterns depicted by MDT-ALES are consistent with the circulation features of the Mediterranean Sea (Poulain et al., 2012; Pinardi et al., 2015). Fig 4.6 depicts a schematic diagram of the surface geostrophic circulation in the Mediterranean Sea which may be useful to follow features of mean circulation discussed hereafter. The following analysis makes reference to the features observed both in the MDT-ALES map and in the VEL-ALES map of velocities.

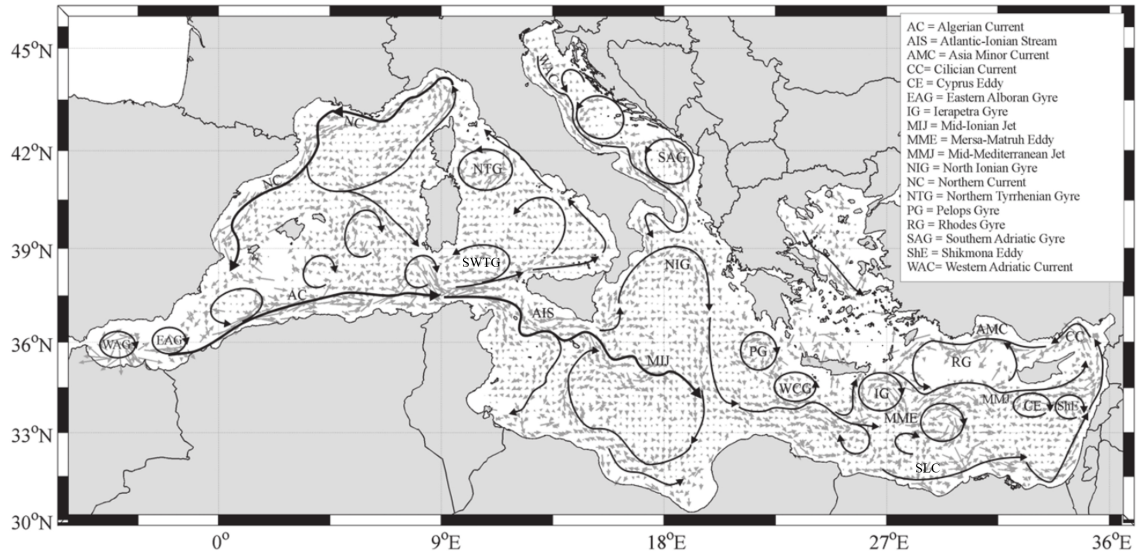


Figure 4.6: Schematic diagram of the surface geostrophic circulation in the Mediterranean Sea. Reproduced from Poulain et al. (2012).

Accordingly to the inflow of Atlantic Water (AW) at the Strait of Gibraltar, a gradient of MDT is found in the Alboran sea between the Spanish and African coasts. The wide absolute minimum of the MDT-ALES near the Provencal coast may be identified with the Gulf of Lion Gyre (GLG). However, compared to the gyre depicted by the SMDT-MED-2014, it extends further south toward the Algerian Sea, and is formed by a single instead of double cell. Moreover, the MDT-ALES

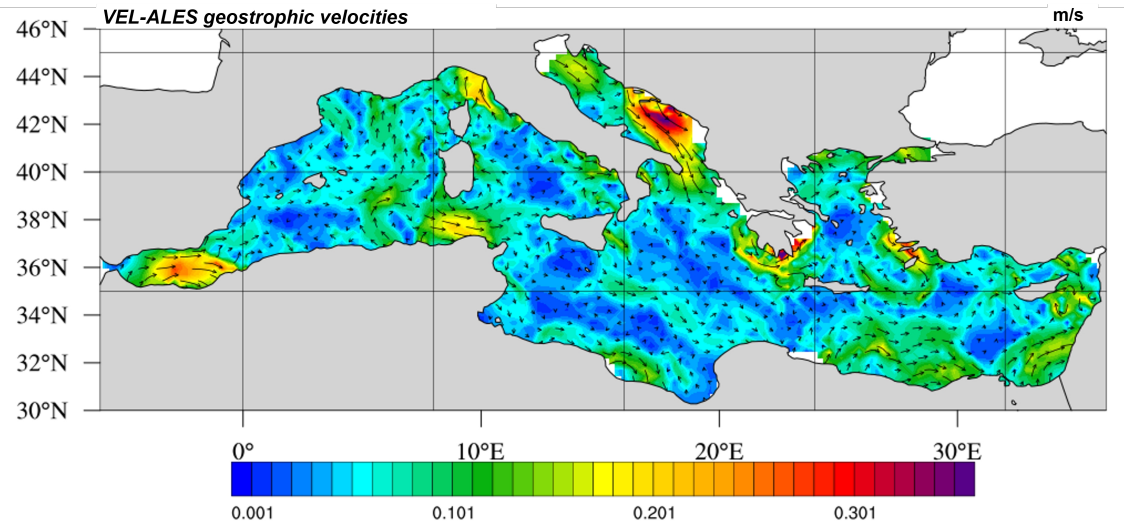


Figure 4.7: Geostrophic velocities derived from the MD-ALES map.

do not "close" the GLG circulation at coast, totally missing the representation of the Northern Current (NC). A relative minimum of the MDT-ALES is seen near the south-eastern corner of Sardinia, corresponding to the South Western Tyrrenian Gyre (SWTG). As for the GLG, the current in the SWTG doesn't flow parallel the coast of Sardinia but is instead perpendicular to it. In the Sardinia channel, a strong north-south gradient of MDT induces an intense eastward flow which is consistent with the Southern Sardinian Current (SSC). Intensities of the AW inflow (≈ 30 cm/s), the GLG ($\approx 10\text{-}15$ cm/s) and of the SSC (≈ 20 cm/s) are comparable with those resulting from other studies (Poulain et al., 2012; Menna et al., 2013). In the Ionian Sea, a basin wide gradient in the MDT-ALES, going from Greece to the African coasts, depicts a southeastward meandering current identifiable with the Atlantic Ionian Stream (AIS). The AIS intensity in VEL-ALES is ≈ 15 cm/s which also agrees with results reported by Poulain et al. (2012). The flow proceeds into the Levantine sea, forming a broad and intense eastward current which occupies the middle/southern part of the basin. This pattern is found where the free open ocean Mid-Mediterranean Jet (MMJ) and the coastal Southern Levantine Current (SLC) are observed. A broad relative minimum of the MDT-ALES located south-east of Crete may characterise the area of Levantine Intermediate Water (LIW) formation. However, this pattern is displaced with respect to the known position of the Rhodes Gyre (RG) (e.g., Poulain et al., 2012).

Despite some large scale patterns of circulation have been identified (AW inflow, GLG, SWTG, AIS, MMJ), many unlikely structures characterise the MDT-ALES map. Small and mesoscale permanent features are displaced or not visible in the MDT-ALES map. This is the case of the Alboran Gyres (AG), which are represented

3. Discussion

as a single broad pattern, and the RG, which is weak and displaced. In addition, other gyres are totally missing, like for instance the Northern Tyrrenian Gyre (NTG) and the Ierapetra Gyre (IG). In the central part of the Levantine sea, the complex system of cyclonic eddies is just outlined by a broad minimum in MDT-ALES. Coastal currents like the NC, the Algerian Current (AC), the Asia Minor Current (AMC) are not represented in the MDT-ALES. The weak coastal current forming the cyclonic circulation in the southern Adriatic sea is totally misinterpreted by the MDT-ALES. This area is instead characterised by an unreal circulation structure with a single outflow originated within the sub-basin, with currents stronger than 30 cm/s. In many areas, isolines of the MDT-ALES (i.e. current streamlines) are pointing toward or having origin from the coast.

4.3 Discussion

Long wave signals in the difference between the MDT-ALES and the SMD-MED-2014 are observed. These are an offset and a longitudinal gradient. It may be argued that the offset is caused by the assumption of an arbitrary zero level for the computation of the model first guess used to compute the SMDT-MED-2014. Conversely, the MDT-ALES, based on observations, have a basin mean consistent with the mean sea level in other oceans. However, some studies computing the MDT for the Mediterranean Sea with the direct method calculated a basin average close to zero (Woodworth et al., 2015; Menna et al., 2013). Nevertheless, these studies differ from the present work because they use multission MSSH products, generated accomplishing intercalibration between altimeters which may modify the mean signal.

Discrepancies between the MDT-ALES and the SMDT-MED-2014 may arise induced by the set of altimetric corrections applied to compute MDT-ALES. As pointed out in subsection 3.1.1, the Dynamic Atmosphere Correction (DAC), which removes the influence of atmospheric pressure on the level of the sea surface, was not applied in the computation of MDT-ALES. Conversely, the effect of atmospheric pressure is not present in the SMDT-MED-2014, which is based on MFS reanalysis obtained before this forcing was introduced in the model (Adani et al., 2011; Oddo et al., 2014). Therefore variations in sea surface height induced by atmospheric pressure are included in the MDT-ALES but not in the SMDT-MED-2014. In Fig 4.8 we display the along track values of the DAC averaged over the 2008-2015 period. This height, subtracted to the MDT-ALES, would remove the influence of atmospheric pressure. We see that this correction would coherently offset the

MDT-ALES toward zero and contrast the gradient observed in Fig 4.5b. However, both the DAC offset and gradient amplitudes (respectively 5 cm and 10 cm from the westernmost to the easternmost extreme of the basin), are not enough to compensate the differences between the MDT-ALES and the SMDT-MED-2014 (respectively 30 cm and 40 cm). Therefore, the origin of the large scale differences between the MDT-ALES and the SMD-MED-2014 is still unknown.

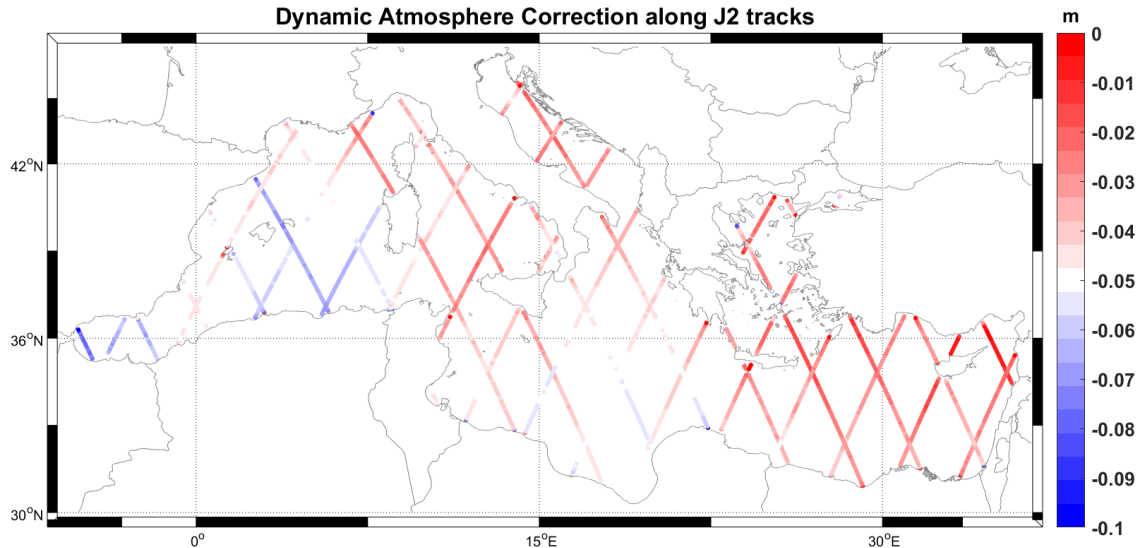


Figure 4.8: Along track values of the Dynamic Atmosphere Correction averaged over the 2008-2015 period.

Differences between MDT-ALES and SMDT-MED-2014 at the sub-basins scale might be induced by multi-year variability, since the two MDTs are referred to different periods. Bonaduce et al. (2016) analysis shows that the Mediterranean sea level variability is composed by high frequency as well as low frequency components (seasonal, intra-annual, processes that have dominant periodicities of about 10 years); moreover a residual trend was found for the period 1993-2012, which presents marked spatial variability. Large variations in gyres location and current amplitudes over multi-years periods interest mostly the Alboran sea, the Ionian basin, the Cretan passage and the Levantine basin (Poulain et al., 2012; Pinardi et al., 2015). All the above considerations may in part explain the small and mesoscale differences between MDT-ALES and SMDT-MED-2014 visible in Fig 4.5b most of all in the Alboran Sea and Levantine basin.

Another reason for inaccuracies in the MDT-ALES is the spatial distribution of J2 observations. Small and even mesoscale features are left almost unsampled due to the large distance between J2 satellite tracks. An emblematic case is the absence of the RG, which is not depicted by the MDT-ALES, although its permanent character, because is placed in between J2 tracks (Iudicone et al., 1998); RG position with

3. Discussion

respect to J2 tracks, to the east of Crete, is visible in Fig 4.5a. For the same reason the NTG is also not detected by the MDT-ALES. Pascual et al. (2007) show that the low spatial resolution of the Jason series of satellites is completely insufficient for mesoscale studies, while at least three satellites with complementary coverage are required for a correct monitoring of the mesoscale activity in the Mediterranean Sea.

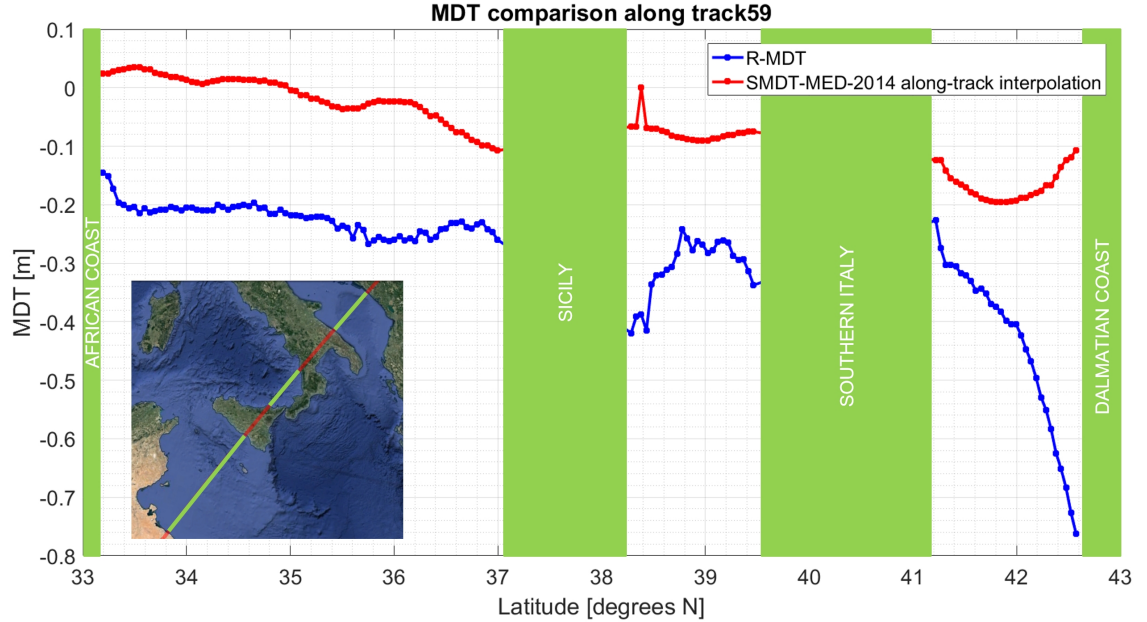


Figure 4.9: Comparison of R-MDT and SMDT-MED-2014 interpolated along track 59 from the African to the Dalmatian coasts. An unexpected steep gradient is visible in the R-MDT.

The distance between J2 tracks in part explains why most coastal currents are not represented by the MDT-ALES. However, they are missing also in areas covered by multiple J2 tracks (see for instance in the area of the NC current). Fig 4.2 confirms that they are not even captured by the along track R-MDT: the signature of the GLG along track 146 is visible in the SMDT-MED-2014, which presents a minimum near the French coast, but not in R-MDT, which decreases monotonically. On the contrary, in other cases, such as along track 59, crossing the southern Adriatic, the R-MDT presents unexpected coastal steep gradients, resulting in unlikely intense flows. (Fig 4.9). Since incorrect representation of coastal MDT features is observed even in the along track MDT, we could attribute some unlikely elements of MDT-ALES either to altimetry or geoid model inaccuracy. The altimetric dataset was however evaluated in subsection 3.2.2, and demonstrated good agreement with the TAPAS SLA dataset. Hence, we hypothesise that inaccuracies of R-MDT at coast are due the fact that the geoid model cannot follow coastal steep gradients of bottom

3. Discussion

topography in regions of sudden and frequent transition between land and ocean.

The reconstruction of the two dimensional MDT field from R-MDT observations by mean of OA introduces further inaccuracies at coast. Since the interpolation grid extends over lands, and OA does not take into account topographic constraints, currents result to be unrealistically perpendicular to the coasts in most of the Mediterranean.

Chapter 5

Conclusions and Outlooks

In this thesis, an altimetric Coastal Geophysical Data Record (CGDR) retracked near the coasts with a dedicated algorithm (ALES, i.e. the Adaptive Leading Edge Subwaveform retracker) has been used to compute a Mean Dynamic Topography (MDT) map for the Mediterranean sea. The MDT and the derived geostrophic velocities were analyzed in order to assess the induced circulation around the basin in a qualitative way. Firstly, the ALES dataset was used to build up homogeneous time series of Sea Surface Height (SSH) along Jason 2 satellite (J2) tracks, through a co-location process. This dataset was then used to compute an along track Mean SSH (MSSH). The high resolution geoid model EGM2008 was then subtracted from the MSSH to reconstruct the Mediterranean MDT along J2 tracks. Finally, an optimal interpolation algorithm was used to spread MDT values on a homogeneous two-dimensional horizontal grid covering the whole Mediterranean Sea.

Results showed that altimetric data retracked by ALES algorithm, along with dedicated editing and selection implemented in this work, can successfully retrieve SSH observations close to the coast (order of a couple of kilometres) in the Mediterranean Sea. ALES derived R-SLA dataset, compared to the MFS operational TAPAS SLA dataset, revealed a more complete time series and a comparable standard deviation within most of the basin. An increased amount of observations was found in some coastal areas, i.e. in the Alboran sea, around the southern Italian coasts and in the Aegean sea. Areas of high sea level variability were correctly located by the ALES dataset (Alboran and Algerian seas, Ionian and Levantine basins).

The MDT map reconstructed from the ALES dataset and the EGM2008 geoid model showed different accuracy depending on the considered scale. The MDT-ALES map well reproduced at basin scale the meridional gradient induced by the typical double gyre structure of the Mediterranean circulation. Wide and intense

circulation patterns could be recognized, such as, from west to east, the Atlantic water influx at Gibraltar, the Gulf of Lion Gyre, the Southern Sardinia Current, the Atlantic Ionian Stream and the Mid Mediterranean Jet. Conversely, our results did not properly reconstruct small and mesoscale features as well as coastal currents. Many mesoscale eddies are not visible or displaced in the MDT-ALES, and circulation often do not close at coast, flowing instead perpendicular to it. Hence, one of our main objectives, the evaluation of the Mediterranean sea dynamics by means of recently reprocessed altimetry, has been only partially achieved.

One reason for this are some unrealistic MDT features observed in the along track estimates (see 4.3). A source of this inaccuracy can be found either in the altimetric SSH dataset or in the geoid model. Since altimetry was validated against an external product with good results, we assume that these small scales of circulation couldn't be well captured by geoid resolution.

Future investigation on the along track MDT sensitivity to the geoid model are needed. Woodworth et al. (2015) use, in the Mediterranean, the GOCO03S 'Extended' (GOCE COmbed) and the GOCE release DIR5 'Extended' models, combinations of GOCE geoid, improved with information from the EGM2008. In the Norwegian Sea (Ophaug et al., 2015), the use of global geoid models improved with regional terrestrial gravity data provided by the Norwegian Mapping Authority gave very good results. However, error level in state of the art geoid models like GOCE at scales below 100 km is still high compared to the Mediterranean oceanic signal variance, and filtering should be applied. Combined models using GOCE can improve the representation of large scale features (around 100 km) but not the small scales (or the coastal areas).

Another reason for incomplete reconstruction of Mediterranean dynamics is due to J2 satellite sampling not dense enough to capture the small and mesoscale features. Pascual et al. (2007) demonstrated that three or four satellites are needed to properly map the mesoscale gyres in the Mediterranean Sea. Important circulation features like the Rhodes Gyre are not observed by J2 tracks spaced more than 200 km, as corroborated also by our results in chapter 4. We can infer that a multi-mission dataset is required for a complete representation of Mediterranean circulation, dominated by mesoscale features.

Therefore we suggest that future developments of the present work include at least three satellites with complementary spatial coverage. The choice of satellites must compromise between the optimal arrangement of their ground tracks and the compatibility of their operational periods. We could suggest, taking as reference Pascual et al. (2007) and Pujol et al. (2010), the satellites combination Jason-1,

ERS2 (or Envisat), TOPEX/Poseidon interleaved and Geosat Follow-On. In addition, since the integration of multiple satellites data results in considerably big datasets, the approach could initially be tested on limited areas.

Other secondary improvements could be considered in order to further reduce unrealistic features near the coasts, for example:

- substitute the standard altimetric corrections with corrections specifically designed to have enhanced performances near the coasts (e.g. tidal harmonic components computed by Birol et al. (2017), sea state bias recomputed using retracked altimetric parameters);
- regrid along track MDT observation through an optimal interpolation technique which takes into account topographic and dynamic constraints, in order to decouple sub basins so that data influence does not cross lands (e.g. Troupin et al., 2012).

Appendix A

Range and Geophysical Corrections

Troposphere and Ionosphere refractive effects

The range which would be observed if the radiation was travelling through the vacuum is given by $R_{corr} = c \cdot \tau/2$, where c is the speed of light in the free space and τ is the two-way travel time of the radar pulse. The speed of a signal within a non-dispersive medium (such as the troposphere can be considered) is related to the real part of its refractive index, n_r , i.e. it's linked to its transmittance t_λ . Figure 2.6 shows the transmittance of subpolar (dotted line), midlatitude (solid line) and tropical (dashed line) cloud-free atmospheres at normal incidence angle as a function of frequency in the microwave band 1-300 GHz; altimeter Ku- and C-band frequencies (13.6 Ghz and 5.3 Ghz) are chosen for their high transmittance, respectively around 96% and 98%.

In a more general case of dispersive medium travel time and path length are related by $dz = \frac{c}{n} \cdot dt$, where n is the complex refractive index, so finally the difference between the actual range and the range estimated from measurements through a medium is given by:

$$\Delta R = R_{corr} - R_{obs} = c \cdot \tau/2 - \frac{1}{2} \int_0^\tau \frac{c}{n} \cdot dt = \frac{c}{2} \cdot \int_0^\tau \frac{n-1}{n} \cdot dt = 10^{-6} \int_0^R N(z) \cdot dz \quad (\text{A.1})$$

where in the last equivalence we call $N(z) = 10^6(n(z)-1)$ the refractivity, which substituted to n because for the microwave band the index of refraction is nearly 1. The integrated refractivity can be then seen as the sum of various contributions in the atmosphere, namely the dry tropospheric refractivity N_{dry} associated with dry

gases, the water vapor refractivity N_{vap} , the cloud liquid water droplet refractivity N_{liq} , and the ionospheric refractivity N_{ion} .

Dry tropospheric correction

The optical thickness, hence the refractivity $N(z)$, of troposphere is related to its density ρ_a , which is given by the contribution of ‘dry gases’ (mostly constituted by oxygen) and water vapour. Dry gases are much denser than water vapour so the troposphere density is given in first approximation by $\rho_a \approx \rho_{dry}$. Path delay induced by the presence of dry gases is then proportional to the vertically integrated density profile, which is linked by hydrostatic approximation to the ratio between Sea Level Pressure (SLP) and the gravity constant (expressed below as a function of latitude):

$$\Delta R_{dry} \propto \int_0^R \rho_{dry}(z) \cdot dz \approx P_0/g_0(\theta) \approx P_0 \cdot (1 + 0.0026 \cos(2\theta)) \quad (\text{A.2})$$

Since direct observations of SLP are infrequent and scarcely distributed, gridded pressure fields provided operationally by numerical weather prediction models, like the ECMWF, are generally used. Dry troposphere correction corresponds to a decrease in observed range of about 225-235 cm, and is by far the largest of range corrections. Long spatial scales of variability of dry gas content with respect to the wet component means that this correction is relatively unaffected by the presence of land (Andersen and Scharroo, 2011). It has been already adopted for other coastal studies (Jesus et al., 2016) and will be used in this work.

Wet tropospheric correction (WTC)

Wet components of the atmosphere include water vapour, cloud droplets and rain.

Water vapour and cloud droplets, whose effect is taken in account by WTC, are distributed throughout the troposphere much more irregularly than the dry gases (Ruf et al., 1994) so their hydrostatic contribution to refraction can be considered negligible. Water vapour refractivity main contribution can be expressed as proportional to the ratio of its partial pressure and the squared temperature (Smith and Weintraub 1953); assuming linearity of $T(z)$ in the lower 10 km and replacing the surface temperature with an effective temperature T_{eff} to absorb some of the error from neglecting variation of T with height, water vapour path delay can be written as:

$$\Delta R_{vap} \propto \int_0^R \frac{P_{vap}(z)}{T(z)^2} \cdot dz = \int_0^R \frac{\rho_{vap}(z)}{T(z)} \cdot dz \approx \frac{1}{T_{eff}} \int_0^R \rho_{vap}(z) \quad (\text{A.3})$$

Much weaker is the effect of cloud droplets, which is proportional to the integrated columnar liquid water content:

$$\Delta R_{liq} \propto L_z \quad (\text{A.4})$$

WTC hence rely on the measurement of the atmospheric total water content, which for its high variability in space and time is not suitable to be computed with high accuracy by interpolation of numerical weather prediction models. Simultaneous estimates need to be accomplished, derived by on board passive radiometers measuring the atmospheric brightness temperature near the water vapor line at 22.24 GHz and providing suitable removal of the background. In the OSTM/Jason-2 Microwave Radiometer (AMR) the water vapor signal is sensed by the 23.8 GHz channel, while the 34 GHz channel removes cloud cover influence (Keihm et al., 1995). Since GDR-D product version the algorithm implemented by Brown (2010) is applied to radiometer measurements, which accounts for errors in the correction retrieval near the coasts due to land contamination.

Due to their dimensions raindrops absorbs and scatter radiation in the microwave band much more with respect to the other wet components of the troposphere. Moreover rain events are usually smaller than the footprint of radar signal, influencing the shape of the returned waveform, which ends in a biased estimation of altimeter parameters (Monaldo and Goldhirsh, 1986). This makes it impossible to retrieve useful information in these cases and therefore measurements contaminated by the presence of rain are usually flagged as bad and eliminated. This process is not however straightforward and techniques to identify rain events have been suggested (Tournandre and Morland, 1997). Despite the efforts, flags in some cases miss the detection or falsely discard good data due to an incorrect rain detection algorithm, being at present not well implemented in Jason 2 GDR products (Thithonis and Achuthan, 2013). Jason 2 data records include two rain flags: one based on both dual-frequency altimeter and AMR measurements and another only on AMR measurements. As the former removes a portion of coastal measurements with a suspiciously homogeneous pattern, which would constitute a limitation in our case, the flag based on AMR measurements has been chosen.

Ionospheric correction (IC)

The ionospheric range correction for a given frequency f is fully determined from knowledge of the Total Electron Content (TEC) along the path of radar pulse prop-

agation:

$$\Delta R_{ionp} \propto \frac{1}{f^2} \int_0^R n_e(z) \cdot dz = \frac{TEC}{f^2} \quad (\text{A.5})$$

Because this effect is dispersive the dual-frequency altimeter allows its estimation measuring the range at two different frequencies. Two different solutions included in Jason 2 GDR for this correction adopt this technique: in one case, along-track simultaneous estimate of TEC is derived from the analysis of waveform returned to the satellite; in the other, TEC is computed by a ground network of GPS receivers which detect the dual-frequency signal sent from multiple satellites and interpolate the TEC content on Global Ionospheric Maps (GIM). Some studies (Ho et al. (1997), Jee et al. (2010)) show that the average difference between GIM and TOPEX/Poseidon estimates of TEC values is very small (less than 1.5 TEC units, corresponding roughly to a difference in the correction of about 2 cm) within 2000-km distances from the GPS stations. At present hundreds of stations worldwide are available, mostly distributed in the northern hemisphere. Hence over the Mediterranean GIM solution offers the advantage of a performance comparable to the simultaneous estimates, further adding continuity in coastal regions, where the along-track simultaneous solution has instead a low performance due to altimetric waveform corruption. Using the smooth GIM solution allows to concentrate our study on the performance of altimeter retracking.

Sea state bias correction

Within the altimeter footprint the sea surface distribution is not gaussian, being wave peaks much more rare than troughs; moreover the latters backscatter a greater amount of power per unit area normal to the surface. This induce differences between the actual mean sea level and the mean scattering surface, and between the mean and the median of scattering surface, that is actually measured by the onboard tracker. Both these effects can be expressed in terms of the Significant Wave Height, which is defined as the higher third of the wave heights.

$$\Delta R_{SSB} \propto SWH \quad (\text{A.6})$$

SWH is extracted directly from the altimeter waveform, which is why this correction depends on the specific retracking algorithm. Other studies show that the sea state bias correction recomputed in limited regions using ALES algorithm improves the quality of the retrieved sea level (Jesus et al., 2016). Since the full recomputation along all Mediterranean tracks is not yet a public product (personal communication

with Passaro) the correction derived by the standard MLE4 retracking of waveforms has been used in this work.

Tides corrections

Tidal induced variation of the sea surface can be divided in four main contributions: ocean tide, loading tide, solid earth tide and polar tide. The ocean tide, load tide and solid earth tide are related to the direct and indirect luni-solar forcing of the earth; pole tide is due to variations in the Earth's rotation.

The solid earth tide and the pole tide are very well known processes which are normally described using closed mathematical formulas. Their derivation and accuracy can be found respectively in Cartwright and Tayler (1971) and Cartwright and Edden (1973) and in Wahr (1985).

The ocean tide describes the direct effect of gravitational attraction of heavenly bodies on the ocean water masses while the loading tide account for the indirect effect of water mass loading on the bottom topography. Ocean tide signal constitutes the dominant effect and is responsible for more than the 80% of total signal variance in most regions (Andersen and Scharroo, 2011). The period of the diurnal and semi-diurnal constituents (the most energetic ones) is much higher than the repetitiveness of satellite cycles, and cannot be resolved in altimeter observations, consequently aliasing to the lower frequencies that are of interest for oceanographic studies (Ablain and Zawadzki, 2016). Considerable efforts have been undertaken within the ocean tide community to correct these aliasing errors, particularly in the latest versions of Global Ocean Tide (GOT, computed by Goddard/NASA) and Finite Element Solution (FES, computed by LEGOS/NOVELTIS/CLS) models.

Correction for ocean and loading tide included in the Jason 2 data records files is the sum of all the diurnal and semidiurnal ocean and load tides as predicted by GOTv4.8 and an equilibrium representation of the long-period ocean tides at all periods except for the zero frequency (constant) term.

The removal of the here described effects needs to be carefully evaluated in relation to the specific oceanographic application where the satellite data are used. For instance when comparing with tide gauges measurements the direct effect of gravitational attraction on water mass is the only to be retained in the altimeter measurements, since the other three effects are not sensed with respect to the bottom fixed platforms.

Since tides are not yet implemented in the MFS this correction is here applied to altimetric observations.

Dynamic Atmosphere Correction (DAC)

The effect of atmospheric loading on altimetric observations is generally represented as an hydrostatic Inverse Barometer (IB). The Dynamic Atmosphere Correction (DAC) account for additional high frequency variation in atmospheric pressure due to winds at surface and other effects.

In the case of semi enclosed basins as Mediterranean Sea, the response to atmospheric pressure differs from the pure IB because the slow water exchange between the Mediterranean and the Atlantic through the narrow Gibraltar Strait often generates large-scale oscillations that can last for several days (Oddo et al., 2014). Dobricic et al. (2012) shows that, when the MFS model is forced by the atmospheric pressure, the assimilation of uncorrected satellite data set leads to the most accurate analyses. Therefore the DAC correction is not applied here for SSH computation.

Acknowledgements

I would like first of all to thank my supervisor Prof. Nadia Pinardi for guiding me through this work, always carrying positive energy and a smile. Thanks also to Jenny Pistoia, patiently supporting all my steps and helping me to refine the results. A special thank to Paolo Cipollini, who introduced me to satellite altimetry and always found a moment to dedicate to my questions, refreshing time after time my enthusiasm for joining the international scientific community.

I am grateful I've had the chance to participate to the Med-MFC group meetings at INGV, where I learned a lot about scientific and operational discussions. A big thank to Benedicte Lemieux, who showed genuine interest and support for my research in a moment when I deeply needed it.

Thanks to all the great people I met in Bologna during these years: my course-mates (Barbara, Federica, Anna, Luca, Enrico, Matteo), all the flatmates I've shared my craziness with (a special hug to Claudia and Elena), the guys of the Unibo Choir, and those of the fantastic (!) ReSpirale Teatro company, and last but absolutely not least all the people in the '80s/'90s room (and surroundings) at INGV. They made me feel always at home and made me live this city in lot of different ways.

A particular thought to the Fantastic4 girls (Barbara, Federica, Anna), our common interest in science and nature, our common experience of great women in a world of men, made me feel a great affinity with you in so little time. On the other hand, I want to thank those friends who never let me go and always asked for news, despite all the years and the different cities; I'm talking about Damiano and Giulia.

Here we are to *mi Rompi* Sinhuè, with whom at first I discovered myself and then I climbed over all the barriers of space and time to discover us. Thanks for showing me how to push the boundaries with imagination and tenderness.

Alla mia famiglia (Claudia, Fabrizio e Lorenzo, e anche la famiglia allargata), dedico la parte più importante di questa tesi, le ultime righe. Grazie per la fiducia e la partecipazione, la vostra capacità di accettare chi sono e cosa faccio e il vostro entusiasmo per la vita vi renderà sempre miei amici.

Bibliography

- Ablain, M. and Zawadzki, L. (2016). Error Characterization Report: Altimetry Measurements Errors at Climate Scales. Technical Report 30.
- Adani, M., Dobricic, S., and Pinardi, N. (2011). Quality Assessment of a 1985–2007 Mediterranean Sea Reanalysis. *Journal of Atmospheric and Oceanic Technology*, 28(4):569–589.
- Andersen, O. B. and Scharroo, R. (2011). Range and geophysical corrections in coastal regions: And implication for mean sea surface determination. In Vignudelli, S., Kostianoy, A. G., Cipollini, P., and Benveniste, J., editors, *Coastal Altimetry*, pages 103–145. Springer.
- Anzenhofer, M., Shum, C. K., and Rentsh, M. (1999). Coastal Altimetry and Applications. Technical Report 464, Department of Civil and Environmental Engineering and Geodetic Science, The Ohio State University.
- Bingham, R. J., Haines, K., and Lea, D. J. (2014). How well can we measure the ocean’s mean dynamic topography from space? *Journal of Geophysical Research: Ocean*, 119(6):3336–3356.
- Birol, F., Fuller, N., Lyard, F., Cancet, M., Niño, F., Delebecque, C., Fleury, S., Toublanc, F., Melet, A., Saraceno, M., and Léger, F. (2017). Coastal applications from nadir altimetry: Example of the X-TRACK regional products. *Advances in Space Research*, 59:936–953.
- Bonaduce, A., Pinardi, N., Oddo, P., Spada, G., and Larnicol, G. (2016). Sea-level variability in the Mediterranean Sea from altimetry and tide gauges. *Climate Dynamics*, 47(9-10):2851–2866.
- Bouffard, J., Roblou, L., Birol, F., Pascual, A., Fenoglio-Marc, L., Cancet, M., Morrow, R., and Ménard, Y. (2011). Introduction and assessment of coastal altimetry strategies: case study over the northwestern mediterranean sea. In

- Vignudelli, S., Kostianoy, A. G., Cipollini, P., and Benveniste, J., editors, *Coastal Altimetry*, chapter 12, pages 297–330. Springer.
- Bourassa, M. A., Gille, S. T., Jackson, D. L., Roberts, J. B., and Wick, G. A. (2010). Ocean winds and turbulent air-sea fluxes inferred from remote sensing. *Oceanography*, 23(4):36–51.
- Brown, G. (1977). The average impulse response of a rough surface and its applications. *IEEE Transactions on Antennas and Propagation*, 25(1):67–74.
- Brown, S. (2010). A Novel Near-Land Radiometer Wet Path-Delay Retrieval Algorithm: Application to the Jason-2/OSTM Advanced Microwave Radiometer. *IEEE Transaction on Geoscience and Remote Sensing*, 48(4):1986–1992.
- Candela, J. and Lozano, C. J. (1994). *Barotropic response of the western Mediterranean to observed atmospheric pressure forcing*, chapter 15, pages 325–359. Number 46 in Coast. Estuar. Stud. American Geophysical Union.
- Cartwright, D. E. and Edden, A. (1973). Corrected Tables of Tidal Harmonics. *Geophysical Journal International*, 33(3):253–264.
- Cartwright, D. E. and Tayler, R. J. (1971). New Computations of the Tide-generating Potential. *Geophysical Journal International*, 10(1):45–73.
- Chang, Y.-C., Tseng, R.-S., Chu, P. C., and Shao, H.-J. (2016). Global Energy-saving Map of Strong Ocean Currents. *Journal of Navigation*, 69(01):75–92.
- Chelton, D. B., Ries, J. C., Haines, B. J., Fu, L.-L., and Callahan, P. S. (2001). *Satellite Altimetry*, pages 1–132. Academic Press.
- Cipollini, P., Passaro, M., and Snaith, H. M. (2015). ALES Coastal Geophysical Data Records (CGDR) User Handbook. Technical report, National Oceanography Centre.
- Cipollini, P. and Snaith, H. M. (2015). A short course on Altimetry. In *4th ESA Advanced Training on Ocean Remote Sensing*. National Oceanography Centre.
- Coppini, G., Marra, P., Lecci, R., Pinardi, N., Cretì, S., Scalas, M., Tedesco, L., DampapospAnca, A., Fazioli, L., Olita, A., Turrisi, G., Palazzo, C., Aloisio, G., Fiore, S., Bonaduce, A., Kumkar, Y. V., Ciliberti, S. A., Federico, I., Mannarini, G., Agostini, P., Bonarelli, R., Martinelli, S., Verri, G., Lusito, L., Rollo, D., Cavallo, A., Tumolo, A., Monacizzo, T., Spagnulo, M., Sorgente, R., Cucco,

- A., Quattrocchi, G., Tonani, M., Drudi, M., Nassisi, P., Conte, L., Panzera, L., Navarra, A., and Negro, G. (2017). SeaConditions: a web and mobile service for safer professional and recreational activities in the Mediterranean Sea. *Natural Hazards and Earth System Sciences*, 17(4):533.
- Davidson, F., Allen, A., Brassington, G., Breivik, Ø., Daniel, P., Kamachi, M., Sato, S., King, B., Lefevre, F., and Sutton, M. (2009). Applications of GODAE ocean current forecasts to search and rescue and ship routing. *Oceanography*, 22(3):176–181.
- Delrosso, D., Clementi, E., Grandi, A., Tonani, M., Oddo, P., Ferruzza, G. G., and Pinardi, N. (2016). Rapporti tecnici INGV. Towards the Mediterranean Forecasting System MyOcean V5: numerical experiments results and validation. Technical Report 345, Istituto Nazionale di Geofisica e Vulcanologia.
- Demirov, E., Pinardi, N., Fratianni, C., Tonani, M., Giacomelli, L., and De Mey, P. (2003). Assimilation scheme of the Mediterranean Forecasting System: operational implementation. *Annales Geophysicae*, 21(1):189–204.
- Dibarbour, G., Schaeffer, P., Escudier, P., Pujol, M.-I., Legeais, J. F., Faugere, Y., Morrow, R., Willis, J. K., Lambin, J., Berthias, J. P., and Picot, N. (2012). Finding Desirable Orbit Options for the “Extension of Life” Phase of Jason-1. *Marine Geodesy*, 35(S1):363–399.
- Dobricic, S. (2005). New mean dynamic topography of the Mediterranean calculated from assimilation system diagnostics. *Geophysical Research Letters*, 32(L11):1–5.
- Dobricic, S., Dufau, C., Oddo, P., Pinardi, N., and Rio, M.-H. (2012). Assimilation of SLA along track observations in the Mediterranean with an oceanographic model forced by atmospheric pressure. *Ocean Science*, 8(5):787–795.
- Dobricic, S. and Pinardi, N. (2008). An oceanographic three-dimensional variational data assimilation scheme. *Ocean Modelling*, 22:89–105.
- Dobricic, S., Pinardi, N., Adani, M., Bonazzi, A., Fratianni, C., and Tonani, M. (2005). Mediterranean Forecasting System: An improved assimilation scheme for sea-level anomaly and its validation. *Quarterly Journal of the Royal Meteorological Society*, 131(613):3627–3642.
- Dobricic, S., Pinardi, N., Adani, M., Tonani, M., Fratianni, C., Bonazzi, A., and Fernandez, V. (2007). Daily oceanographic analyses by Mediterranean Forecasting System at the basin scale. *Ocean Science*, 3(1):149–157.

Dohan, K. (2017). Ocean surface currents from satellite data. *Journal of Geophysical Research: Oceans*, 122:2647–2651.

Dumont, J. P., Rosmorduc, V., Carrere, L., Picot, N., Bronner, E., Couhert, A., Desai, S., Bonekamp, H., Scharroo, R., Lillibridge, J., and Leuliette, E. (2016). OSTM/Jason-2 Products Handbook. Technical report, CNES-EUMETSAT-NASA/JPL-NOAA/NESDIS.

Ezer, T., Mellor, G. L., Ko, D.-S., Sirkes, Z., and Le Grand, P. (1993). A Comparison of Gulf Stream Sea Surface Height Fields Derived from Geosat Altimeter Data and Those Derived from Sea Surface Temperature Data. *Space Science Review*, 10(1):76–87.

Gommenginger, C., Tibaut, P., Fenoglio-Marc, L., Quartly, G., Deng, X., Gòmez-Enri, J., Challenor, P., and Gao, Y. (2011). Retracking altimeter waveform near the coasts. In Vignudelli, S., Kostianoy, A. G., Cipollini, P., and Benveniste, J., editors, *Coastal Altimetry*, pages 61–101. Springer.

Ho, C. M., Wilson, A. J., Mannucci, A. J., Lindqwister, U. J., and Yuan, D. N. (1997). A comparative study of ionospheric total electron content measurements using global ionospheric maps of GPS, TOPEX radar, and the Bent model. *Radio Science*, 32(4):1499–1512.

Iudicone, D., Santoleri, R., Marullo, S., and Gerosa, P. (1998). Sea level variability and surface eddy statistics in the Mediterranean Sea from TOPEX/POSEIDON data. *Journal of Geophysical Research: Oceans*, 103(C2):2995–3011.

Jee, G., Lee, H. B., Kim, Y. H., Chung, J. K., and Cho, J. (2010). Assessment of GPS global ionosphere maps (GIM) by comparison between CODE GIM and TOPEX/Jason TEC data: Ionospheric perspective. *Journal of Geophysical Research*, 115(A10):1–11.

Jesus, G.-E., Paolo, C., Passaro, M., Vignudelli, S., and Coca, J. (2016). Coastal Altimetry Products in the Strait of Gibraltar. *IEEE Transaction on Geoscience and Remote Sensing*, 54(9):5455–5466.

Jordi, A., Ferrer, M. I., Vizoso, G., Orfila, A., Basterretxea, G., Casas, B., Álvarez, A., Roig, D., Garau, B., Martínez, M., Fernández, V., Fornés, A., Ruiz, M., Fornós, J. J., Balaguer, P., Duarte, C. M., Rodríguez, I., Alvarez, E., Onken, R., Orfila, P., and Tintoré, J. (2006). Scientific management of Mediterranean coastal zone: A hybrid ocean forecasting system for oil spill and search and rescue operations. *Marine Pollution Bulletin*, 53(5-7):361–368.

- Keihm, S. J., Janssen, M. A., and Ruf, C. S. (1995). TOPEXPoseidon Microwave Radiometer (TMR): 111. Wet Troposphere Range Correction Algorithm and Pre-Launch Error Budget. *IEEE Transaction on Geoscience and Remote Sensing*, 33(1):147–161.
- Knudsen, P. and Andersen, O. B. (2013). The DTU12MDT global Mean Dynamic Topography and ocean circulation model. In *ESA Living Planet Symposium*.
- Kourafalou, V. and Tsiaras, K. (2007). A nested circulation model for the North Aegean Sea. *Ocean Science*, 3(1):1–16.
- Le Grand, P. (2002). Impact of geoid improvement on ocean mass and heat transport estimates. *Space Science Review*, 108(1-2):225 – 238.
- Le Traon, P. Y., Nadal, F., and Ducet, N. (1998). An Improved Mapping Method of Multisatellite Altimeter Data. *Journal of Atmospheric and Oceanic Technology*, 15:522–534.
- Levitus, S., Antonov, J. I., Boyer, T. P., and Stephens, C. (2001). *World Ocean Database 1998*. Natl. Oceanic and Atmos. Admin., Silver Spring, Md.
- Marullo, S., Nardelli, B. B., Guarracino, M., and Santoleri, R. (2007). Observing the Mediterranean Sea from space: 21 years of Pathfinder-AVHRR sea surface temperatures (1985 to 2005): re-analysis and validation. *Ocean Science*, 3(2):299–310.
- Menna, M., Poulain, P.-M., and Mauri, E. (2013). Mean surface geostrophic circulation of the Mediterranean Sea estimated from GOCE geoid models and altimetric mean sea surface: initial validation and accuracy assessment. *Bollettino di Geofisica Teorica ed Applicata*, 54(4):347–365.
- Mercier, F., Rosmorduc, V., Carrere, L., and Thibaut, P. (2010). Coastal and Hydrology Altimetry product (PISTACH) handbook. Technical Report 1, CNES.
- Monaldo, F. M. and Goldhirsh, J. (1986). Altimeter height measurement error introduced by the presence of variable cloud and rain attenuation. *Journal of Geophysical Research*, 91(C2):2345–2350.
- Oddo, P., Adani, M., Pinardi, N., Fratianni, C., Tonani, M., and Pettenuzzo, D. (2009). A nested Atlantic-Mediterranean Sea general circulation model for operational forecasting. *Ocean Science*, 5:461–473.

Oddo, P., Bonaduce, A., Pinardi, N., and Guarnieri, A. (2014). Sensitivity of the Mediterranean sea level to atmospheric pressure and free surface elevation numerical formulation in NEMO. *Geoscientific Model Development*, 7(6):3001–3015.

Oke, P. R., Larnicol, G., Jones, E. M., Kourafalou, V., Sperrevik, A. K., Carse, F., Tanajura, C. A., Mourre, B., Tonani, M., Braxton, G. B., Le Henaff, M., Halliwell, G. R., Atlas, R., Moore, A. M., Edwards, C. A., Martin, M. J., Sellar, A. A., Alvarez, A., De Mey, P., and Iskandarani, M. (2015). Assessing the impact of observations on ocean forecasts and reanalyses: Part 2, Regional applications. *Journal of Operational Oceanography*, 8(sup1):s63–s79.

Ophaug, V., Breili, K., and Gerlach, C. (2015). A comparative assessment of coastal mean dynamic topography in Norway by geodetic and ocean approaches. *Journal of Geophysical Research: Oceans*, 120(12):7807–7826.

Pascual, A., Pujol, M.-I., Larnicol, G., Le Traon, P.-Y., and Rio, M.-H. (2007). Mesoscale mapping capabilities of multisatellite altimeter missions: First results with real data in the Mediterranean Sea. *Journal of Marine Systems*, 65(1-4):190–211.

Passaro, M., Cipollini, P., and Benveniste, J. (2015). Annual sea level variability of the coastal ocean: The Baltic Sea - North Sea transition zone. *Journal of Geophysical Research: Ocean*, 120(4):3061–3078.

Passaro, M., Cipollini, P., Vignudelli, S., Quartly, G. D., and Snaith, H. M. (2014). ALES: A multi-mission adaptive subwaveform retracker for coastal and open ocean altimetry. *Remote Sensing of Environment*, 145:173–189.

Pavlis, N. K., Holmes, S. A., Kenyon, S. C., and Factor, J. K. (2012). The development and evaluation of the Earth Gravitational Model 2008 (EGM2008). *Journal of Geophysical Research: Solid Earth*, 117(B4):1–38.

Pettenuzzo, D., Large, W. G., and Pinardi, N. (2010). On the corrections of ERA-40 surface flux products consistent with the Mediterranean heat and water budgets and the connection between basin surface total heat flux and NAO. *Journal of Geophysical Research*, 115(C6):1–15.

Pinardi, N., Allen, I., Demirov, E., De Mey, P., Lascaratos, A., Le Traon, P.-Y., Maillard, C., Manzanella, G., and Tziavos, C. (2003). The Mediterranean ocean forecasting system: first phase of implementation (1998–2001). *Annales Geophysicae*, 21:3–20.

- Pinardi, N. and Coppini, G. (2010). Operational oceanography in the Mediterranean Sea: the second stage of development. *Ocean Science*, 88:395–406.
- Pinardi, N. and Flemming, E., editors (1998). *The Mediterranean Forecasting System Science Plan*. Number 11 in EuroGOOS Publication.
- Pinardi, N., Lyubartsev, V., Cardelluccio, N., Caporale, C., Ciliberti, S., Coppini, G., De Pascalis, F., Dialti, L., Federico, I., Filippone, M., Grandi, A., Guideri, M., Lecci, R., Lamberti, L., Lorenzetti, G., Lusiani, P., Macripo, C. D., Maicu, F., Mossa, M., Tartarini, D., Trotta, F., Umgieser, G., and Zaggia, L. (2016). Marine Rapid Environmental Assessment in the Gulf of Taranto: a multiscale approach. *Natural Hazards and Earth System Sciences*, 16(12):2623–2639.
- Pinardi, N. and Masetti, E. (2000). Variability of the large scale general circulation of the Mediterranean Sea from observations and modelling: a review. *Palaeogeography, Palaeoclimatology, Palaeoecology*, 158:153–173.
- Pinardi, N., Zavatarelli, M., Adani, M., Coppini, G., Fratianni, C., Oddo, P., Simoncelli, S., Tonani, M., Lyubartsev, V., Srdjan, D., and Bonaduce, A. (2015). Mediterranean Sea large-scale low-frequency ocean variability and water mass formation rates from 1987 to 2007: A retrospective analysis. *Progress in Oceanography*, 132:318—332.
- Poulain, P. M., Barbanti, R., Font, J., Cruzado, A., Millot, C., Gertman, I., Griffa, A., Molcard, A., Rupolo, V., Le Bras, S., and de la Villeon, L. P. (2007). MedArgo: a drifting profiler program in the Mediterranean Sea. *Ocean Science*, 3(3):379–395.
- Poulain, P.-M., Menna, M., and Mauri, E. (2012). Surface Geostrophic Circulation of the Mediterranean Sea Derived from Drifter and Satellite Altimeter Data. *Journal of Physical Oceanography*, 42(6):973–990.
- Pujol, M. I., Dobricic, S., Pinardi, N., and Adani, M. (2010). Impact of Multialtimeter Sea Level Assimilation in the Mediterranean Forecasting Model. *Journal of Atmospheric and Oceanic Technology*, 27(12):2065–2082.
- Rio, M. H., Guinehut, S., and Larnicol, G. (2004). A mean dynamic topography computed over the world ocean from altimetry, in situ measurements, and a geoid model. *Journal of Geophysical Research*, 109(C12):1–19.
- Rio, M. H. and Hernandez, F. (2011). New CNES-CLS09 global mean dynamic topography computed from the combination of GRACE data, altimetry, and in situ measurements. *Journal of Geophysical Research*, 116(C7):1–25.

Rio, M. H., Pascual, A., Poulaïn, P. M., Menna, M., Barceló, B., and Tintoré, J. (2014). Computation of a new mean dynamic topography for the Mediterranean Sea from model outputs, altimeter measurements and oceanographic in situ data. *Ocean Science*, 10(4):731–744.

Roblou, L., Lamouroux, J., Bouffard, J., Lyard, F., Le Henaff, M., Lombard, A., Marsaleix, P., De Mey, P., and Birol, F. (2011). Post-processing altimeter data toward coastal applications and integration into coastal models. In Vignudelli, S., Kostianoy, A. G., Cipollini, P., and Benveniste, J., editors, *Coastal Altimetry*, chapter 9, pages 217–246. Springer.

Roblou, L., Lyard, F., Le Henaff, M., and Maraldi, C. (2007). X-track, a new processing tool for altimetry in coastal oceans. *2007 IEEE International Geoscience and Remote Sensing Symposium*.

Ruf, C. S., Keihm, S. J., Subramanya, B., and Janssen, M. A. (1994). TOPEX/POSEIDON microwave radiometer performance and in-flight calibration. *Journal of Geophysical Research*, 99(C12):915–926.

Siegismund, F. (2013). Assessment of optimally filtered recent geodetic mean dynamic topographies. *Journal of Geophysical Research: Oceans*, 118(1):108–117.

Thithonis, M. A. and Achuthan, J. (2013). Validation Study on Jason-2 Rain Flag and Rain Rate Estimation Over North Indian Ocean. *IEEE Geoscience and Remote Sensing*, 10(6):1537–1541.

Tonani, M., Oddo, P., Korres, G., Clemanti, E., Dobricic, S., Drudi, M., Pistoia, J., Guarnieri, A., Romaniello, V., Girardi, G., Grandi, A., Bonaduce, A., and Pinardi, N. (2014). The Mediterranean Forecasting System: recent developments. *Geophysical Research Abstracts*, 16.

Tonani, M., Pinardi, N., Dobricic, S., Pujol, I., and Fratianni, C. (2008). A high resolution free surface model of the Mediterranean Sea. *Ocean Science*, 4(1):1–14.

Tonani, M., Pinardi, N., Fratianni, C., Pistoia, J., Dobricic, S., Pensieri, S., de Alfonso, M., and Nittis, K. (2009). Mediterranean Forecasting System: forecast and analysis assessment through skill scores. *Ocean Science*, 5(4):649–660.

Tournandré, J. and Morland, J. C. (1997). The Effects of Rain on TOPEX/Poseidon Altimeter Data. *IEEE Transaction on Geoscience and Remote Sensing*, 35(5):1117–1135.

- Troupin, C., Barth, A., Sirjacobs, D., Ouberrous, M., Brankart, J. M., Brasseur, P., Rixen, M., Alvera-Azcárate, A., Belounis, M., Capet, A., Lenartz, F., Toussaint, M. E., and Beckers, J.-M. (2012). Generation of analysis and consistent error fields using the Data Interpolating Variational Analysis (DIVA). *Ocean Modelling*, 52–53:90–101.
- Vergos, G. S., Bayoud, F. A., Sideris, M. G., and Tziavos, I. N. (2001). High Resolution Geoid Computation by Combining Shipborne and Multi-Satellite Altimetry Data in the Eastern Mediterranean Sea. *A paper presented at the XXVI General Assembly of the European Geophysical Society (EGS), March 26th–30th, Nice, France.*
- Wahr, J. M. (1985). Deformation Induced by Polar Motion. *Journal of Geophysical Research*, 90(B11):9363–9368.
- Woodworth, P. L., Gravelle, M., Marcos, M., Woppeleman, G., and Hughes, C. W. (2015). The status of measurement of the Mediterranean mean dynamic topography by geodetic techniques. *Journal of Geodesy*, 89(8):811–827.
- Younis, J., Anquetin, S., and Thielen, J. (2008). The benefit of high-resolution operational weather forecasts for flash flood warning. *Hydrology and Earth System Sciences*, 12(4):1039–1051.